Masterthesis

Production and characterization of chromium(III)-doped, dry-mixed UOX pellets

PROMOTOR :
Prof. dr. Sonja SCHREURS

PROMOTOR :   COPROMOTOR :

Ph.D. Rémi DELVILLE   ing. Koen VANAKEN

Jens Van Nerum
Scriptie ingediend tot het behalen van de graad van master in de industriële wetenschappen: nucleaire

technologie, afstudeerrichting nucleaire technieken / medisch nucleaire technieken

Gezamenlijke opleiding UHasselt en KU Leuven

UHASSELT   KU LEUVEN

UHASSELT   KU LEUVEN

2019•2020
Faculteit Industriële ingenieurswetenschappen
master in de industriële wetenschappen: nucleaire technologie

Masterthesis
Production and characterization of chromium(III)-doped, dry-mixed UOX pellets

PROMOTOR :

Prof. dr. Sonja SCHREURS

PROMOTOR :

Ph.D. Rémi DELVILLE

COPROMOTOR :

ing. Koen VANAKEN

Jens Van Nerum
Scriptie ingediend tot het behalen van de graad van master in de industriële wetenschappen: nucleaire technologie, afstudeerrichting nucleaire technieken / medisch nucleaire technieken

Table of contents

List of figures

List of abbreviations

ADU   Ammonium di-uranate

AUC   Ammonium uranyl carbide

BET   Brunauer-Emmet-Teller

EPMA   Electron probe micro-analysis

FGR   Fission gas release

IDR   Integrated dry route

PCI   Pellet-Cladding interaction

STA   Simultaneous Thermal Analysis

TGA   Thermogravimetric analysis

XRD   X-ray diffraction

Abstract (English)

To obtain a higher burn-up, modern nuclear fuel pellets are doped. One such dopant is chromium(III), usually added as chromium(III) oxide. The aim of this study was to produce and characterize uranium pellets doped with chromium(III) oxide.

To this end, we have created several sintered pellet batches starting from Integrated Dry Route (IDR) UO_2 powder, doped with increasing amounts of Cr_2O_3 (0 to 3000 ppm). The sintering kinetics, average grain size and lattice constant of these pellets were examined. A limited amount of pellets were also produced from UO_2 powder obtained via the Ammonium Di-Uranate (ADU) production route. For both type of UO_2 powder mixtures, pellets sintered with a slower temperature profile were also produced.

The main conclusion is that a very fine dispersal of the initial chromium(III) is key to producing homogeneous, large grain size pellets. Currently, EPMA measurements confirm that chromium(III) oxide ends up heterogeneously dispersed inside the pellets, and inhomogenous crystal grain sizes are also observed.

Overall, average crystal grain sizes up to 33 ± 6 µm are observed, an increase of about 200% compared to undoped uranium oxide pellets, though still below the original target of 50 µm. While this number has already been achieved and surpassed by other studies, even higher grain sizes can be reached through optimization of the sintering parameters, better milling and improvements of the starting powders.

Abstract (Nederlands)

Om een hogere burn-up te bereiken worden moderne brandstofpellets gedopeerd. Een mogelijk doperingsmiddel is chroom(III), wat gewoonlijk wordt toegevoegd als chroom(III)oxide, Cr_2O_3. Het doel van dit onderzoek was het produceren van en het bepalen van de eigenschappen van uranium pellets gedopeerd met chroom(III)oxide.

Tijdens dit onderzoek werden verschillende batches van Integrated Dry Route (IDR) UO_2 brandstofpellets gedopeerd met verschillende concentraties aan Cr_2O_3 (van 0 tot 3000 ppm). Van deze pellets werd het sinterprofiel, de gemiddelde kristalgrootte en de roosterparameter onderzocht. Een beperkte hoeveelheid pellets werd ter vergelijking ook geproduceerd vanuit Ammonium Di-Uranaat (ADU) UO_2 poeder. Ook werden enkele pellets met een langzamer sinterprofiel geproduceerd.

Onze bevindingen zijn dat een fijne verdeling van het chroom(III)oxide in de pellet uiterst belangrijk is om een homogene pellet met grote kristallen te produceren. Momenteel wordt door EPMA metingen bevestigd dat de chroom(III)oxide niet homogeen doorheen de pellet wordt verdeeld. Tevens werd waargenomen dat de kristalgroei ook inhomogeen verlopen is.

Gemiddelde kristalgroottes tot 33 ± 6 µm werden bereikt, een stijging van 200% in vergelijking met ongedopeerd uranium oxide, maar toch onder het vooropgestelde doel van 50 µm. Andere studies hebben deze grootte geëvenaard en al verbroken, maar bij ons proces kan de gemiddelde kristalgrootte zeker nog verhoogd worden door verbetering en optimalisatie van o.a. het sinterproces, het malen en de startpoeders.

1. Introduction

In recent years, nuclear fuel manufacturers like Westinghouse, Framatome and Global Nuclear Fuel have announced new series of fuel pellets which are doped with certain metals. These doped pellets have improved physical properties when compared to undoped uranium fuel, which allows for higher burnup cycles. As reactor downtimes are expensive, a longer fuel cycle would result in a reduction of operating costs. These doped pellets are marketed as Enhanced Accident Tolerant Fuels (EATF) and are planned to be deployed by 2025 [1], [2].

Besides reducing operating costs, these doped pellets are also designed to be more resistant to accidents. One possible failure mode is fuel rod cracking due to Stress Corrosion Cracking (SCC). This allows coolant from the reactor to come into direct contact with the fuel itself, which contaminates the coolant. Two possible processes that can lead to degradation of the cladding, the protective cover around the fuel, have been identified. These processes are Pellet-Cladding Interaction (PCI) and Fission Gas Release (FGR). The combination of PCI and FGR is thought to be responsible for SCC. EATF pellets are designed to be resistant to SCC.

As these pellets will eventually reach the end of their life cycle, the European Union has started the *Modern Spent Fuel Dissolution and Chemistry in Failed Container Conditions* project (DisCo). DisCo aims to study the behavior of these doped pellets during the back-end of their fuel cycle, i.e. long-term underground storage. The DisCo project is planned to run from 2017 to 2021. The SCK·CEN, an institution focused on nuclear research near the town of Mol in Belgium, is part of this research project and has been tasked with manufacturing and delivering doped fuel pellets on a laboratory scale [3].

One possible element for doping is chromium(III), usually added as Cr_2O_3 or $Cr(NO_3)_3$. Killeen et al. [4] and Kashibe and Une [5] investigated the FGR of chromium doped pellets, noting an increase in FGR for noble gases at lower burn-up, but a reduced FGR at higher burn-up when comparing Cr_2O_3 doped fuel to undoped fuel. Killeen also noted an increase in crystal grain size for chromium(III) oxide doped pellets. Bourgeois et al. [6], [7] investigated the effect of chromium(III) oxide on grain growth in UO_2 fuel, noting again an increase in crystal grain size. They attributed this to the formation of a $Cr-Cr_2O_3$ eutectic. Additional research [8–10] has attempted to determine the solubility limit of chromium(III) oxide in UO_2, finding values in the 700-900 ppm range. This solubility limit is strongly dependent on sintering conditions and the O/U ratio of the uranium oxide used.

The effects of chromium(III) doping, added as chromium(III) oxide (Cr_2O_3), on depleted (less than 0.7% U-235) uranium fuel are examined. The main point of interest is to obtaining a detailed graph of resulting crystal grain size in function of added concentration of chromium(III) oxide. Additionally, the effect of the origin of the uranium oxide (synthesized from Ammonium Di-Uranate (ADU) or synthesized by the Integrated Dry Route (IDR) process) are compared. Finally, the sintering kinetics of the resulting powder mixtures are compared.

2. Literature study

2.1 Anatomy of a fuel rod

Fuel is added to a nuclear reactor as a "fuel rod". A diagram of such a rod is shown in figure 1. The actual fuel part of the rod consists of fuel pellets. Fuel pellets are small cylinders of pressed and sintered powder fuel material. This material is usually either uranium dioxide (UOX) or a mixture of uranium and plutonium oxides (MOX). The dimensions of a single pellet are only a few millimetres, both in height and in diameter. The complete fuel rod can be several meters tall, housing hundreds of pellets stacked on top of each other. Surrounding the pellets is the cladding of the fuel rod. The cladding is often a zirconium alloy, as zirconium has a low cross section for neutrons, but some fuel rod designs use a stainless steel cladding instead. The drawback of using zirconium is that zirconium is more susceptible to chemical attack from fission products than stainless steel. Before irradiation, there is a gap between the pellets and the cladding. During irradiation, the pellets expand to fill this gap.
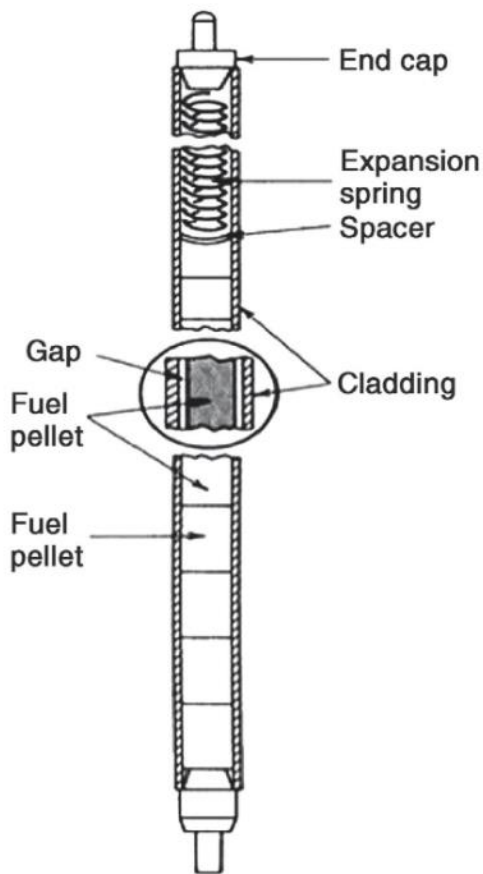
Figure 1: Schematic of a light-water fuel rod. Source: [11]

2.2 Pellet-cladding interaction and fission gas release

The swelling of the fuel pellets creates mechanical stresses in the cladding, referred to as PCMI (pellet-cladding mechanical interaction). The effect of PCMI is dependent on many factors, including pellet deformation, ramping speed of the reactor power, reactor holding time and many more. The exact description of the origin and propagation of these stresses is very complex, and is out of the scope of this thesis. A comparison between cladding failure studies can be found in [12] and more recently, in [13].

When the mechanical stresses induced by PCMI are high enough, the cladding can deform and crack. This cracking will first occur in points where the cladding is weaker. This weakening of the cladding can be caused by a pre-existing fault from fuel rod production, or caused by some process resulting from in-pile irradiation. One such process is the presence of decay products resulting from the irradiation. Specifically iodine [14], cesium [15] and cadmium [16] are thought to be responsible for PCI.

Combined with PCI, FGR is another factor that impacts the likelihood of a fuel rod cracking during irradiation. FGR refers to the release of gaseous decay products (Xe, Kr) produced during in-pile irradiation. These tend to diffuse out of the fuel pellets and become trapped in the space between the pellet and fuel rod cladding. Then, during reactor operation, these gases will attempt to expand due to the elevated temperatures in the fuel rod. As free space in the fuel rod is limited, this expansion leads to an increase in pressure and this induces more stresses on the cladding material. One possible solution to reduce FGR is to dope the fuel with chromium(III) oxide. This oxide has been shown to enlarge the crystal grains of the fuel, which increases the diffusion path of fission gases and reduces the FGR at high burn-up. Careful control of production parameters can also lead to a fuel that is slightly porous. These pores are closed off from the outside atmosphere, and they can contain fission gases inside the pellets during reactor operation [4], [17].

2.3 Uranium dioxide conversion routes

After enrichment, uranium is in the UF_6 state. Pellet fabrication processes require the uranium to be in the UO_2 form. There are several processes to turn UF_6 into UO_2 One route is the direct conversion by treating the UF_6 with superheated steam. This route creates no liquid waste, and is referred to as the Integrated Dry Route (IDR) [18].

Another popular route is first treating the UF_6 with steam, then reacting it with ammonia and nitric acid. This reaction yields Ammonium Di-Uranate (ADU). The ADU is converted to UO_2 either by direct reduction with H_2 gas in a furnace, or first oxidized to U_3O_8 and then reduced to UO_2.

A third route is the Ammonium Uranyl Carbonate (AUC) (sometimes also called Uranyl Ammonium Carbonate, UAC) route. Here, the UF_6 is reacted with ammonia and CO_2 to form AUC. It is then reduced to UO_2 at high temperature in a fluidized bed reactor. Other routes exist, such as several sol-gel processes. However, these are not currently used for commercial pellet production and will not be further considered. The conversion to AUC also requires specialized equipment, and will not be considered in this thesis. An overview of the three major conversion routes is given in figure 2 [19].

4
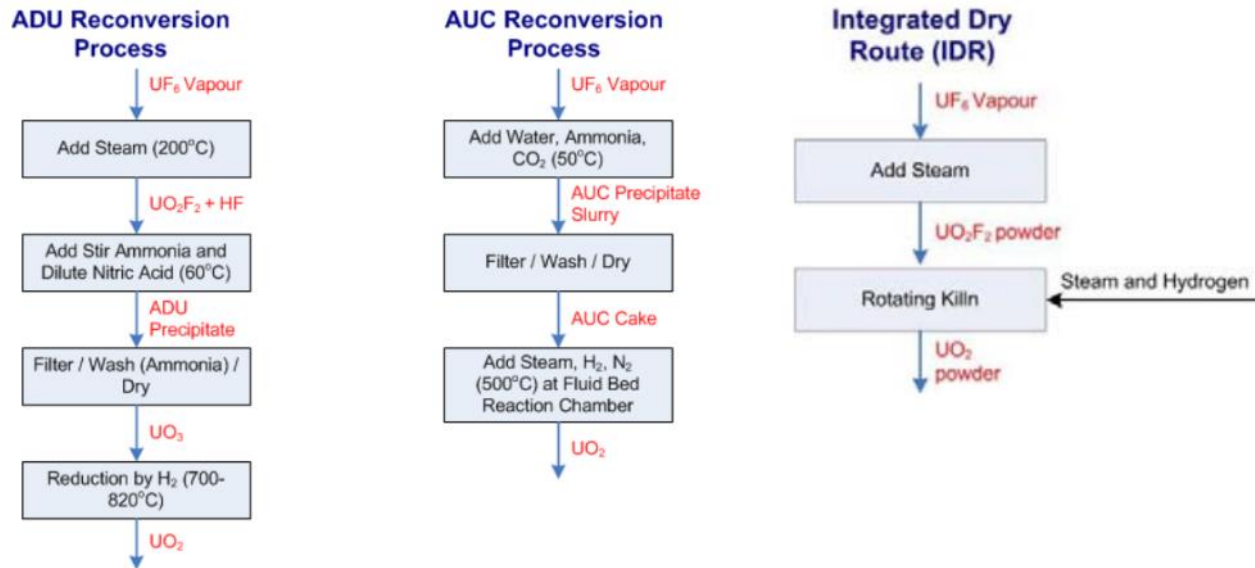
Figure 2: Three common uranium conversion routes. Source: [19]

2.4 Fuel pellet fabrication

2.4.1 Pressing

One of the key properties of the powder for pressing is its flowability. This is influenced by both particle shape and particle sizes present in the powder. A very coarse, round powder flows much better than a very fine, irregular one. This is due to friction among the particles, the smaller these are, the more surface area they have per unit volume. Rounded particles will also have less contact area with each other, and thus, less friction. The chemical species of the particles also plays a large role in the flowability of the powder, as interactions among the particles may be stronger or weaker depending on the chemistry. Additives for use during pressing exist. For example, to improve the flowability of a powder zinc stearate can be added [20], [21].

Another key property is the powder's packing density. This is a measure of how efficiently the particles of the powder fill the available space. This is again influenced by particle shape and particle size distribution. In the theoretical, ideal case, a perfectly stacked spherical powder would fill about 64% of the available space. The remaining 36% is open space and is referred to as pores. Pores can all be interconnected, which is called open porosity, or they can all be closed off little voids in the material, which is called closed porosity. The density of such porous materials is often expressed as a percentage of the theoretical density (%TD) of the material, assuming it has zero porosity. For example, a sintered fuel pellet might have a density of 95 %TD – that is, the pellet weighs 95% of what a solid single-crystal of UO_2 would weigh if it had the same size as the pellet. Other ways of expressing the density of a powder is the apparent density, where a volume of powder is simply poured into a container and weighed, and the tap density which involves tapping on the side of the container to allow the powder to settle before weighing [20], [21].

Pre-pressing, followed by a granulation and spheroidisation is commonly used. The flowability of the powder is increased by the rounded granulates, so it better fills the die and becomes more strongly bound together after pressing. Pre-pressed powders are less likely to develop cracks or pits during

sintering. The flowability is more important for pellet production at an industrial scale, as powder has to be able to flow freely to prevent blockages in dies and machinery.

2.4.2 Sintering

After pressing, the powder is an agglomerate of separate particles, with open porosity among them. This is thermodynamically unfavourable as this configuration has a very large surface area per unit volume and thus a very large surface energy. The surface energy is defined as the amount of energy required to create a certain surface. For example, to cleave a slab of material in half (thus creating two new surfaces), chemical bonds along the cleaving interface need to be broken and this requires energy, which is stored in the surface created. As nature tends to favour states of lower total energy, there will be a tendency of the material to reduce the total surface energy. However, chemical bonds in the bulk of the material prevent atoms from diffusing and reshaping the geometry of the powder to accomplish this reduction [22], [23].

How well a powder sinters is expressed by the powder's sinterability. A powder with a high sinterability can reach a higher density after sintering. The sinterability is dependent on several factors, among which are the flowability and the specific surface area (SSA). In the case of UO_2, the sinterability is quite high – UO_2 can sinter to densities above 97% [20].

The sintering process can be divided into roughly three stages. An image showing these three stages is shown in figure 3. During the first stage, so-called necks form between individual particles. Material flows from the surface of the particles to these necks so they grow in size. This is a very rapid process, because there is a strong driving force to reduce the large surface areas present in non-sintered material. At the end of the first sintering stage, the pores present in the material are all still interconnected and roughly cylindrical in shape. The density of the pellet will slightly increase during this stage [22], [23].
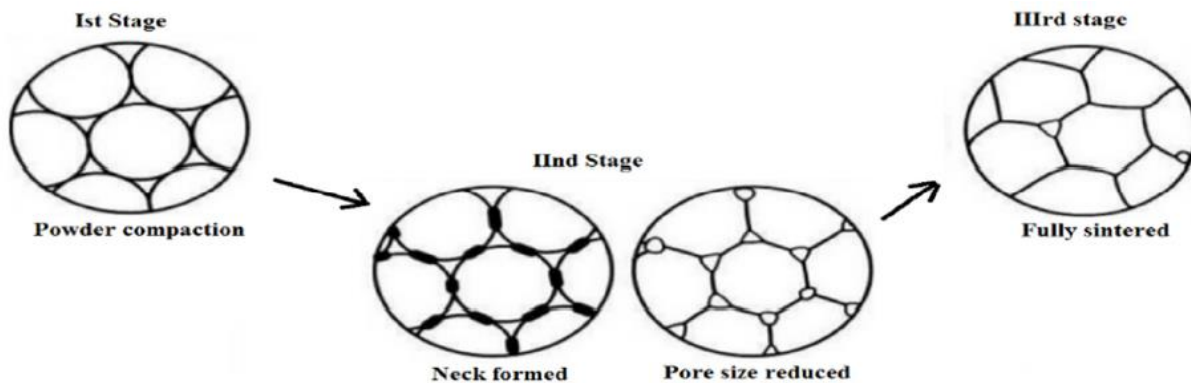
Figure 3: Three stages of sintering, Source: [24]

During the second stage of sintering, the necks have grown large enough to make contact with one another. The interface between two necks will form a grain boundary between the two particles, which are from then on referred to as crystallites. Material will diffuse from the bulk of the pellet towards the grain boundaries, which causes the centres of the crystal grains to move closer together. This causes the entire pellet to shrink and densify. The pores present in the first stage are gradually filled and reduced to cylindrical voids where they previously intersected. At the end of the second stage, connections between pores no longer exist. All pores are isolated and the porosity is closed. At this point, the density of the pellet is about 95 %TD [22], [23].

6

The third and final stage of sintering involves the migration of crystal grain boundaries. Large crystal grains have comparatively less surface area per volume than smaller grains, so they are energetically more favourable. Individual atoms will diffuse across the grain boundary from smaller grains to larger ones. Large crystal grains will thus grow even larger, consuming smaller crystal grains in the process. Pores move with the migrating grain boundary, though exceptionally fast growing crystals can trap a pore inside a grain. Pores will shrink and collapse where possible, as removing them reduces the surface energy. If there is gas trapped in these pores, it will counteract the shrinkage by increasing in pressure. As long as there is gas trapped inside pores, they will not collapse and the density will not reach the theoretical 100 %TD. In the case of uranium oxide the maximum density achievable is about 97-98 %TD [22], [23].

Impurities present during sintering, even in very small concentrations (several hundred ppm) can dramatically influence sintering behaviour. Precipitates of a second, solid phase (i.e. adding chromium(III) above the limit of solubility) can pin the grain boundaries in place. The overall movement of these boundaries will therefore slow down and the area around these precipitates will have smaller crystal grains. Alternatively the additives may increase or decrease the diffusion coefficients of the bulk material, which speeds up or slows down grain growth, respectively. Some additives may form a liquid phase during sintering. Diffusion of material proceeds much faster in liquid phases, thus these additives lead to increased crystal grain size [22], [23].

2.4.3 Sintering atmospheres

To describe the atmosphere used during experiments or sintering, two types of units are commonly used. These are oxygen potential and oxygen partial pressure. They are related by formula (1.1) [25]. Throughout this thesis the oxygen potential will be used to describe the atmosphere.

$$\mu_{O_2} = R \cdot T \cdot \ln(P_{O_2}) \tag{1.1}$$

Here, μ represents the oxygen potential in J/mol, R is the gas constant (8.31 J/mol K), T is the temperature in kelvin and P_{O_2} is the partial pressure of oxygen in the atmosphere, expressed in atm. Other works may report the gas flows used to form the atmosphere, from which the oxygen partial pressure can be calculated. For some experiments, water vapour is also directly added to the atmosphere. The H_2O vapour will dissociate to form an equilibrium with H_2 and O_2. In case the oxygen potential is not supplied for these experiments, the dew point is usually reported instead. This is the temperature at which water vapour condenses from the sintering atmosphere. From the dew point, one can then calculate the partial pressure of H_2O vapour and determine the composition at that temperature. This composition can then be related to the atmosphere at the sintering temperature. From the temperature and enthalpies of the gases present one can then obtain the oxygen potential and oxygen partial pressure of the sintering atmosphere. The sintering atmosphere has major effects on the resulting grain size of doped UO_2, as Cr_2O_3 only has an effect in a limited range of oxygen potentials. For Cr_2O_3 doping it is generally required to stay around -420 kJ/mol, as Cr_2O_3 has little to no impact otherwise [7].

Careful control of the atmosphere when working with UO_2 is always important, as UO_2 is known to readily change its O/U stoichiometry at elevated temperatures. In oxidizing atmospheres, UO_2 will accept additional oxygen atoms as interstitials in its crystal lattice. Conversely, in reducing atmospheres, oxygen is released from the UO_2 lattice, leaving behind vacancies. The physical properties of UO_2 vary strongly depending on stoichiometry [25].

2.5 Chromium(III) oxide dopant

Doping nuclear fuel by adding minute concentrations of metal oxides to the fuel mixture before sintering can have major benefits for the physical properties and in-pile performance of the resulting fuel. Many different dopants exist, and much research has already been published on the characterization of these doped fuels [4], [5], [7]–[10], [26]–[29]. One possible dopant is chromium(III) oxide, or Cr_2O_3. Cr_2O_3 is known to enhance the size of UO_2 crystal grains after sintering [17].

Chromium(III) oxide is a soft, green solid at room temperature and has a melting point of 2 435 °C. The high-temperature behaviour and phase relations of the Cr-O system were examined by Toker et al [30]. They confirmed the presence of a Cr_3O_4 crystal phase at 1650 °C, which appears together with a liquid phase which is assumed to be a eutectic formed between Cr_2O_3 and Cr. This eutectic forms at around 1650 °C, which is attained during sintering. It is therefore possible that dopant chromium(III) oxide forms a liquid phase during the sintering process. This presence of a liquid phase could be beneficial to grain growth. Figures 4 and 5 show data obtained by Toker, though figure 5 has been slightly edited to include oxygen potentials. Figure 4 shows the phase diagram of the Cr-O system. It shows that chromium has several liquid phases, which start forming at 1655 °C. Curiously, Bourgeois [7] reports that the growth-enhancing effect of chromium doping already occurs at temperatures around 1550 °C, well below the eutectic temperature. Figure 6 shows the Ellingham diagram of chromium. This is used to predict whether or not a certain atmosphere will reduce or oxidize chromium at a certain temperature.
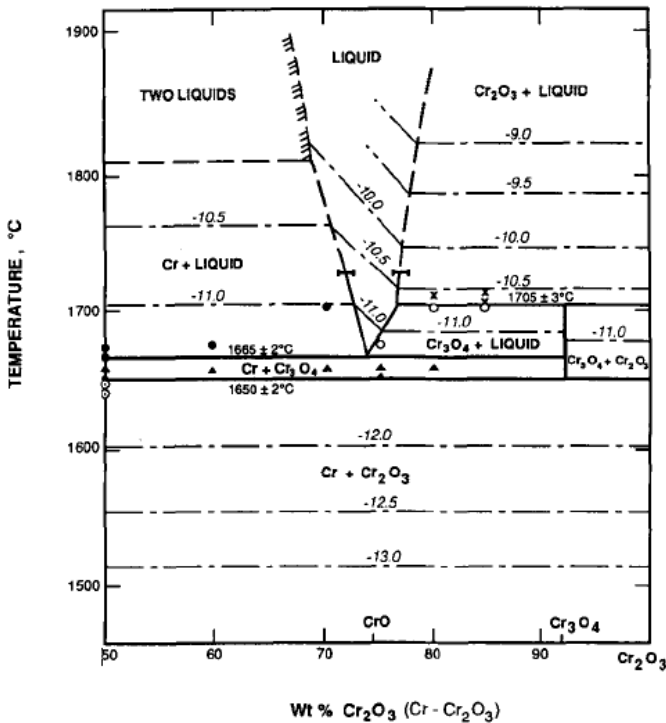
Figure 4: Phase relations in the Cr-O system. Source: [30]
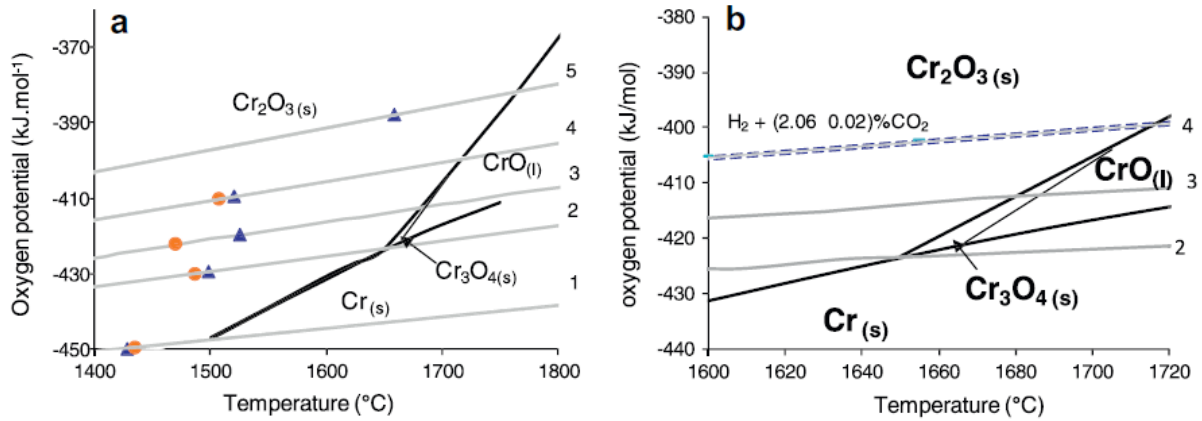
Figure 5: A) Thermal profile of Cr₂O₃, B) Detail showing the CrO(l) phase more clearly. Source: [27]
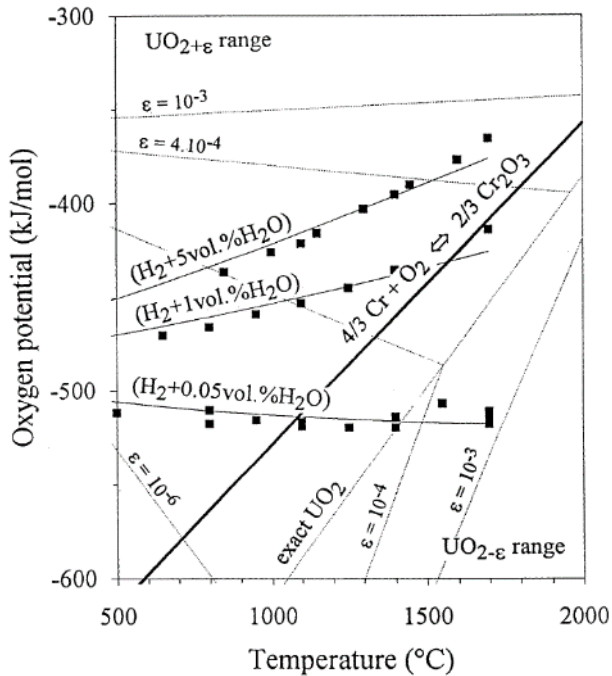
Figure 6: Ellingham diagram of chromium, with some oxygen potentials added. Source: [7]

Cr_2O_3 added as a dopant will dissolve into the UO_2 crystal lattice. According to simulations by Cooper et al [29], the dissolved chromium(III) ends up mostly being incorporated as substitutional defects for uranium atoms in the crystal lattice. This is in agreement with XRD measurements by Cardinaels [8]. They also simulated properties (bond length) of Cr_2O_3-doped uranium, which matches measurements by Mieszczynski [28].

The dissolution of chromium(III) oxide in uranium dioxide has been investigated by Leenaers [10], Kleykamp [31], Bourgeois [6], [7] and Riglet-Martial [9]. The limit of solubility for Cr_2O_3 in UO_2 was found to depend both on temperature and oxygen potential of the surrounding atmosphere. For the parameters used in this thesis (-420 kJ/mol, 1650 °C) this limit is about 0.07 wt.%, or 700 ppm [9]. Any chromium(III) oxide added in excess of this limit will precipitate out to form a second, solid phase. This second phase can pin grain boundaries during sintering, which reduces the overall sintering rate.

The average crystal grain size first increases with increasing chromium(III) oxide content, up to the limit

of solubility. After that, crystal grain size sharply drops, to then rise again towards a second maximum in the 2000-2500 ppm range, depending on temperature. This second rise is possibly due to more liquid chromium(III) being present during sintering, which improves sintering kinetics. The grain size in function of chromium(III) oxide content is shown in figure 7 for several sintering temperatures.

Cooper et al. [29] also found in their simulations that the addition of chromium(III) oxide to uranium dioxide causes an increased amount of defects in the crystal lattice (specifically of the type v_U'''') at elevated temperatures, when compared to undoped uranium oxide. A graph showing defect concentrations is shown in figure 8. These vacancies enhance the diffusion of uranium atoms, which improves the sintering rate. Cooper et al. [29] also state that the improved sintering due to vacancies is responsible for the peak in grain size at the solubility limit of chromium(III) oxide (i.e., 700-900 ppm), while the effect of the eutectic is responsible for the peak at higher concentrations (i.e., >2000 ppm). This would explain the absence of a second peak on the 1525 °C isotherm in figure 7, as that is below the temperature required to form the eutectic.
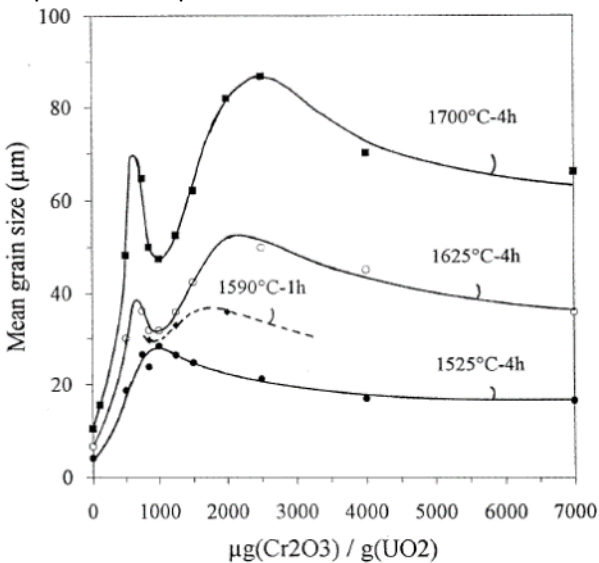
Figure 7: Crystal grain size in function of temperature and chromium content. Source: [7]
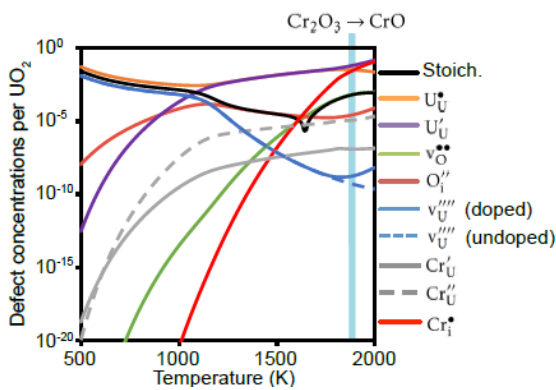
Figure 8: Simulation of various defects present in (doped) UO_2 at an oxygen partial pressure of 10^{-20} atm, which corresponds to an oxygen potential of -740 kJ/mol. Source: [29]

10

2.6 Chromium(III)-doped pellets

The properties of chromium(III)-doped pellets were examined in detail by Bourgeois [6], [7]. Some of the main findings that are also explored in this thesis are added below. All of Bourgeois' measurements are based on IDR-derived uranium powder, with chromium(III) added via spray-drying.

2.6.1 Grain size

The addition of chromium(III) to uranium oxide pellets influences the average crystal grain size of the uranium oxide after sintering. The relation between chromium(III) oxide content and grain size is shown in figure 7. Grains in undoped UO_2 are about 10 μm wide, with the exact size depending on sintering conditions. Adding chromium causes the average grain size to increase drastically, peaking at 750 ppm chromium for all temperatures. The temperature influences the resulting grain size as well, with higher temperatures leading to larger grains. The peak grain size is found to be about 65 μm for 750 ppm Cr_2O_3 at 1700 °C sintering. Adding more chromium(III) oxide causes the average grain size to decrease, up to around 1000 ppm. Further addition of chromium causes the average crystal grain size to increase once more assuming that sintering temperature exceeds 1600°C. The maximum average grain size reached is for 2500 ppm Cr_2O_3 at 1700 °C sintering, which is about 86 μm.

2.6.2 Sintering kinetics

Chromium(III) oxide influences the growth rate of crystals during sintering resulting in larger grain size. Results from two studies are considered in this thesis. These are shown on the left side of figure 9 for Bourgeois' results [7], and on the right side of figure 9 for Peres' results [27]. The powder in Bourgeois' research has been doped with 1000 ppm Cr_2O_3 by spray-drying, while the chromium(III) oxide in Peres' study was added via dry mixing/milling. Both studies agree that chromium(III) oxide-doped pellets require a slightly higher temperature to start sintering, but achieve a much higher densification rate compared to undoped uranium. The sintering kinetics are strongly influenced by the sintering atmosphere, as is illustrated in the differences between Bourgeois' and Peres' results. Additionally, Bourgeois notes that there is a secondary peak in the sintering rate at around 1525 °C. They state that this behaviour is seen regardless of the amount of chromium(III) oxide added, green pellet density or rate of temperature increase. However, it only appears in one specific sintering atmosphere, which is H_2 + 1 vol.% H_2O (approx. -410 kJ/mole at 1700 °C).
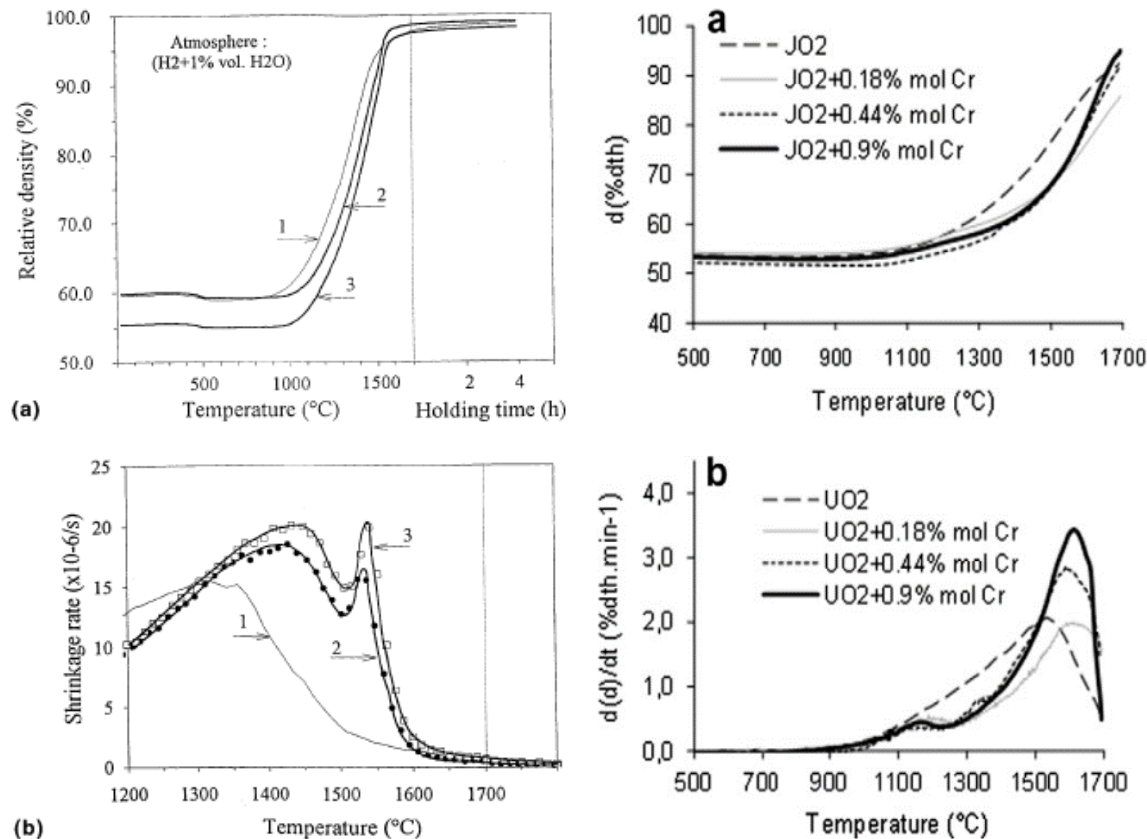
Figure 9: left: Changes in (a) relative density and (b) shrinkage rate for 1) undoped UO_2, 2) spray-dried UO_2 with 1000 ppm Cr_2O_3, pressed at 300 MPa and 3) the same powder, but pressed at 100 MPa. Source: [7] Right: Density (a) and rate of densification (b) during sintering for undoped and Cr-doped UO_2 pellets in $H_2 + 2.06\%$ CO_2 atmosphere. Source: [27]

2.7 Conclusion

Currently, when nuclear fuel pellets are irradiated in a nuclear reactor, there is a very small chance the cladding of the fuel rods cracks. This cracking is the result of two major processes, PCI and FGR. PCI refers to the combined effect of the pellet swelling and chemical attack by fission products produced during irradiation. FGR refers to the release of gaseous fission products, which increase the pressure inside the fuel cladding, which also creates additional stresses.

One possible way to mitigate FGR is to create the fuel pellets in such a way that their average crystal grain size is larger. As the fission gases can only travel along grain boundaries, larger grains would increase the mean distance they have to diffuse to reach the pellet-cladding gap. One possible way to increase the grain size is to dope the uranium fuel with chromium(III) oxide.

The mechanism responsible for creating the enlarged grains is thought to be twofold. First, the formation of a liquid Cr-O eutectic, which increases uranium diffusion, and secondly, an increased amount of uranium vacancies, which also increases uranium diffusion. The increase in the diffusion coefficient of uranium increases the growth speed of crystals during sintering. This leads to enlarged crystal grains.

In this thesis the effect of the origin of the uranium (ADU-based or IDR-based) is examined for several powders, mixed by dry milling. The doping level of chromium(III) oxide is varied, as is the sintering speed.

12

Finished pellets are examined by optical microscopy, XRD and EPMA. The sintering kinetics are categorized with dilatometry. The main goal is to obtain pellets with a main crystal grain size of 50 micron or more.

3. Methods and materials

3.1 Chemicals

3.1.1 UO_2

Origin of the powders

All of the uranium oxide used for pellet fabrication in this study was manufactured by FBFC, a subsidiary of Areva NP, specifically by their plant in Romans-sur-Isère. It was fabricated using the IDR technique. An accompanying document listing the impurities and material properties of this powder can be found in Appendix A. The powder used as a UO_2 reference for BET did not come from this batch. The BET reference is a separate batch, though also fabricated using IDR.

IDR-derived powders

The uranium dioxide was sieved (150 μm sieve opening) before use. Where necessary, the powder was milled as well. As this increases the specific surface area of the powder, a BET measurement was performed after sieving to obtain the new specific surface area of the starting material. It has been assumed to be more or less constant for all sieved IDR-derived uranium dioxide powders. Similarly, the O/U ratio was verified with an STA analysis, as the O/U ratio can change slowly over time and the powder was several years old at time of use. The characterization of this powder can be found in par. 4.1.

ADU-derived powders

The ADU powder used in this study has been synthesized from IDR powder. The details of these syntheses can be found in paragraph 3.2.1. The IDR uranium was dissolved in nitric acid and precipitated with ammonium hydroxide. Next, the solution is centrifuged to separate the ADU uranium from the supernatant. Finally, the resulting ADU cake is left to dry in air. After drying, the powder was milled and sieved (150 μm), similar to the IDR powder.

3.1.2 U_3O_8

U_3O_8 is produced from UO_2 by oxidizing in a Nabertherm muffle furnace (600 °C, 4h, air) for IDR powder. For ADU-based pellets the U_3O_8 was also produced by oxidising ADU UO_2 under the same conditions.

3.1.3 Cr_2O_3

The chromium(III) oxide used in this thesis was supplied by KULeuven. It was originally purchased from Testbourne Ltd and is rated at a 99.8% purity. The Cr_2O_3 powder was milled before use (plastic vial, 3 zirconia milling balls, Turbula), but as it was still rather coarse, it was crushed in a mortar using the back of a spatula before adding to the mixture.

3.1.4 Zinc stearate

Zinc stearate is added as a press lubricant. The powder itself was purchased from VWR international. Like the other powders, it was sieved (150 μm) before use.

3.1.5 Etch materials

The HF used for the etch solution was a 40% concentration bought from Sigma-Aldrich. The HF is diluted 1:3 with water, and 1.5 grams of $Cr(VI)O_3$ are added for every 10 ml of diluted HF solution. The $Cr(VI)O_3$

powder was bought from VWR international, though no purity was known, and the original bottle long disposed.

3.1.6 ADU synthesis materials

The nitric acid used for ADU synthesis has a concentration of 65 wt.%, and was bought from VWR international. The ammonia solution has a concentration of 25 wt.%, and was bought from Sigma-Aldrich.

3.2 Doped fuel pellet synthesis

3.2.1 ADU powder synthesis

Amount of materials listed is for a theoretical maximum yield of 30 grams of ADU UO_2 powder.

First, 30.2133 grams of IDR UO_2 powder and a stir bar are added to a 250 ml Erlenmeyer flask. The 0.2133 additional grams are to compensate for water that adsorbs on the uranium. A 5.33 M solution of HNO_3 is then prepared by adding 20.51 ml of HNO_3 (65 wt. %) to 35.03 ml of demineralized water. The diluted nitric acid is added dropwise to the UO_2 powder. This is done slowly, as the resulting reaction releases significant amounts of heat and NO_2 gas while forming uranyl nitrate. When the reaction slows down, the remaining nitric acid can be added. The uranium is then left to dissolve under heating (50-70 °C) and mild stirring. When everything is dissolved, the solution should be clear and bright yellow in colour. After cooling down, it can be transferred to a sealed container.

A 4 M NH_4OH solution is also prepared, by adding 64.67 ml of 25 wt.% NH_4OH to 39.48 ml of water. Four falcon tubes are placed in a beaker and secured in place with tissue paper. To each tube, a stir bar, approx. 26.04 ml of 4M NH_4OH and approx. 13.89 ml of the uranyl nitrate solution (stepwise, 0.5 ml/step) are added. The ADU should precipitate out, being yellow to dark orange in colour. The tubes are sealed and centrifuged (4000 RPM, 2 min). The supernatant is removed, and the solids are washed with water. It is then centrifuged again. After washing three times, the remaining solids are loosened by adding ethanol and breaking up the mass using a spatula. Everything is then transferred to an evaporation dish and the ethanol is left to evaporate.

After drying, the ADU powder is transferred to a crucible and calcinated in a Nabertherm muffle furnace (air flow, 550 °C for 4 hours) to obtain U_3O_8 and then reduced in a Carbolite tube furnace (Ar/5% H_2, 600 °C, 4 hours) to obtain ADU UO_2 powder.

3.2.2 Pellet production and dopant levels

3.2.2.1 IDR pellets

A total of 14 uranium oxide batches were prepared with different dopant levels between 0 and 3000 ppm Cr_2O_3. The exact dopant levels and the measurements performed on each of the batches can be found below, in table 1. A similar table for ADU pellets is available in table 2. Six of the IDR dopant levels (0, 400, 800, 1200, 1600 and 2000 ppm) have 10 wt.% UO_2 replaced by an equivalent U_3O_8. For the other eight dopant levels (500, 600, 700, 900, 1000, 1100, 2500, 3000 ppm Cr_2O_3), 20 wt.% UO_2 has been replaced by U_3O_8. This was to obtain pellets with a higher porosity, as the first batch of pellets was too dense.

For all these dopant levels, fast sintering has been performed, and all but three of these levels have had pellets etched and the crystal grain size determined. For six dopant levels (0, 400, 800, 1200, 2000, 3000

ppm), slow sintering has been performed, and these pellets have etching and grain size determination planned. For nine dopant levels (0, 500, 700, 800, 900, 1100, 1600, 2000, 3000 ppm), dilatometry has been performed. For all dopant levels, XRD has been performed. EPMA was only performed on the 1000 and 1100 ppm Cr_2O_3 samples.

Table 1: Dopant levels and performed measurements for the IDR pellets (* indicates planned measurements)

dopant level	wt. % U_3O_8	amount of pellets	grain size (fast sintering)	grain size (slow sintering)	dilatometry	XRD	EPMA
0	10	6	X	X*	X	X	
400	10	6	X	X*		X	
500	20	6	X		X	X	
600	20	6	X			X	
700	20	6	X		X	X	
800	10	6	X	X*		X	
900	20	6			X	X	
1000	20	6				X	X
1100	20	6			X	X	X
1200	10	6	X	X*		X	
1600	10	6	X		X	X	
2000	10	6	X	X*	X	X	
2500	20	6	X	X*		X	
3000	20	6	X	X*	X	X	

3.2.2.3 ADU pellets

Six dopant levels were prepared (0, 400, 800, 1200, 1600 and 2000 ppm). All six of these levels have planned examination with XRD, and will have their crystal grain size determined by etching after both slow and fast sintering. All of these pellets contain 20 wt.% U_3O_8. Measurements on these pellets are still pending.

Table 2: Dopant levels and planned measurements of ADU pellets

dopant level	wt. % U_3O_8	amount of pellets	grain size (fast sintering)	grain size (slow sintering)	Dilatometry	XRD	EPMA
0	20	6	X*	X*		X*	
400	20	6	X*	X*		X*	
800	20	6	X*	X*		X*	
1200	20	6	X*	X*		X*	
1600	20	6	X*	X*		X*	
2000	20	5	X*	X*		X*	

3.3 Techniques

3.3.1 Powder mixing/milling
Powders in this study were mixed/milled using a WAB Turbula. Powders are added to a small glass vial together with one methacrylate milling ball. The vial is capped, sealed with duct tape, and placed into a plastic bag. It is then placed in the Turbula for 20 minutes at 72 RPM.

3.3.2 Pellet production
To produce pellets, several quantities of powder are weighed and then homogenized by milling. There are four powders: UO_2, U_3O_8, zinc stearate and Cr_2O_3. The details of these powders can be found in par. 3.1. After homogenizing, pellets are pre-pressed at a pressure of 2-4 kN (approx. 13-26 MPa) in a Komage K6 press. The resulting green pellets are granulated in a Freund Vector rotary granulator with a 20 mesh sieve, then rounded by rolling the granulate at 37 rpm for 40 minutes. More zinc stearate is then added, and the powders are rolled another 12 minutes before final pressing at 15-20 kN (approx. 99-130 MPa) in the Komage press. For final pressing, the filling and target height are varied to obtain a density of about 55 %TD. They are then sintered in a Linn HT-1800-Moly furnace. The final sinter density should be in the 95-97 %TD range.

3.3.3 Sintering conditions
Two sintering profiles are used, one dubbed "fast" and one dubbed "slow". The "slow" sintering heats to 1625 °C with a thermal gradient of 2.5 K/min. The "fast" sintering uses a thermal gradient of 5 K/min. Both hold the 1625 °C plateau for 6 hours. Both also have the same atmosphere of -420 kJ/mol, achieved by mixing 5.1 ml/sec 5% H_2/Ar and 74.9 ml/sec Ar gas flows.

3.3.4 Analysis techniques

3.3.4.1 Immersion density
By measuring the weight of the pellets in air and their weight in water, the density can be accurately determined. Other ways of determining the density exist, such as weighing and measuring the dimensions of a pellet (also called geometric density), though these are less practical as the pellets are not perfect cylinders.

3.3.4.2 BET analysis
The Brunauer-Emmet-Teller (BET) gas adsorption method, is a technique used to determine the specific surface area of a sample, usually a powder. It was named after three scientists who developed a theory describing the monolayered adsorption of gases on surfaces. Despite being named after the theory, the actual BET method is very much an empirical method, with little regard for the theory itself. BET measurements are subject to much variance, and always made with a known standard as a reference.

The measurement itself consists of about a gram of sample being placed in a sample holder. It is then vacuum sealed. The whole sample holder is heated under vacuum to remove any remaining air or moisture inside the sample. Then, it is placed in the BET device. The device will then fill the whole sample holder with He to determine the free volume inside. It is then evacuated once more, and then slowly filled with N_2 while the pressure is recorded. As the whole chamber is kept at liquid N_2 temperatures, N_2 added will adsorb onto the sample. From the behaviour of the pressure curve, one can estimate when

18

the sample is covered by a monolayer of N_2. Then, by making an estimation of the size of a single N_2 molecule, the sample surface can be estimated.

The apparatus used is a TriStar II, from Micromeritics.

3.3.4.3 XRD

X-ray diffraction (XRD), is a technique in which the reflection of X-rays is used to determine the distances between atoms in crystalline samples. Suppose several coherent incident X-rays, all making the same angle θ with the sample. They each interact with the sample, scattering under some angle θ due to Snell's law, but from different crystal planes within the sample. The scattered X-rays will then interfere with one another. If they are all still in phase, they will interfere constructively and they can then be picked up by a detector. Thus, the detector measures a signal only if the additional distance travelled by reflecting from a deeper crystal plane exactly equals some multiple of the X-rays' wavelength. The relation between the distance between crystal planes d, the wavelength λ and the angle θ is given by Bragg's law:

$$\lambda = 2\,d\,\sin\theta \tag{2.1}$$

In our measurements, the X-rays were generated by a copper-nickel tube at 40 kV, 40 mA. The actual XRD machine was a Bruker D8 advance. A monochromator was not available, so reflections from both Cu $K_{\alpha1}$ and Cu $K_{\alpha2}$ are present in the results.

The sample preparation for an XRD measurement consists of immobilizing the pellet and preparing the surface. In this case, the pellet was immobilized in resin. Pellets are embedded in groups of two to three, with a metal plaque in between them. They are then cut in half lengthwise and polished to a mirror finish.

Spectra obtained from the XRD were analysed with PANalytical's X'Pert HighScore Plus software. A known reference spectrum of pure UO_2 was added to select only UO_2 peaks, as the metal plaque from the sample preparation produces unwanted peaks in the spectrum. Next, the displacement of the pellet is calculated and corrected for. Finally, the lattice parameter is calculated from a unit cell refinement with the least squares method. The Smith & Snyder Figure Of Merit (FOM) is also reported. The higher the FOM value, the more reliable the measurement.

3.3.4.4 EPMA

Electron probe micro-analysis (EPMA) is a technique comparable to SEM. It differs from SEM in that it also allows for the analysis of the chemical composition of a microscopic area of a sample. It does this via a very precise electron beam. The electrons interact with atoms present in the sample, exciting them. The excited atoms then fall back to their ground state, emitting characteristic X-rays in the process. These X-rays are filtered based on wavelength and measured by the EPMA device. From the wavelength and intensity of the X-rays both the atom species and concentration can be determined.

The standard mode of operation for an EPMA is a line scan. A pellet is first embedded in resin, then cut in half along the length of the pellet and polished to a mirror finish, similar to XRD pre-treatment. A line is then defined across the sample, in this case lengthwise across the centre line of the pellet. The EPMA will then sample 30 locations at set intervals along this line. For every sampling, the uranium, oxygen and chromium(III) content are reported.

Benedictus Vos suggested to also conduct a mapping scan. Certain data points from the line scan are selected, then a second line scan is conducted at a 90° angle to the first. This results in a 2-dimensional grid of measurements. Two pellets were measured this way, initially containing 1000 and 1100 ppm Cr_2O_3 before sintering.

The EPMA setup used is a CAMECA SX100. It is operated at a voltage of 20 keV, with a current of 200 nA, and a tungsten electron gun.

3.3.4.5 Dilatometry
Dilatometry is the measurement of the expansion or shrinkage of objects under certain conditions. A dilatometer consists of a sample holder inside a tube furnace with a controlled atmosphere. To start a measurement, a sample is first mounted in the sample holder. A push rod then continuously applies a slight force to it, so that any expansion or shrinkage of the sample can be accurately logged. During the measurement, the atmosphere and temperature can be varied.

In our case, the dilatometer is a Netzsch DIL 402C. The dilatometer uses the same atmosphere and sintering profile as the "fast" sintering, i.e., 5 °C/min to 1625 °C, which is held for 6 hours in a -420 kJ/mol atmosphere. There is no special sample preparation required.

3.3.4.6 Simultaneous Thermal Analysis
The STA is a combination of a TGA and a mass spectrometer. The TGA consists of a very sensitive scale in a heated chamber, which is also fitted with a calorimeter. This allows the device to analyse any chemical changes or reactions in a sample during heating. The mass spectrometer functionality of the device is not used for this research, as we do not expect any volatiles components to escape from the UO_2 powder. Additionally, the heat transfer line connecting both components of the STA is not suited to the temperatures associated with sintering.

The STA is a Netzsch STA 449 F1 'Jupiter'.

3.3.4.7 Etching and crystal grain size
To determine the crystal grain size, the samples are first embedded in resin and then cut and polished to a mirror finish. The smooth surface is then etched with a solution of CrO_3 in 10 vol% HF. 1.5 grams of CrO_3 is added for every 10 ml of HF solution. The etch procedure was adapted from the procedure used previously at FBFC Dessel, before they closed. During the initial etching attempt, the embedded pellets are submerged face-down in the etch solution for 40 seconds with movement to dislodge any air bubbles, then thoroughly rinsed with water and finally thoroughly rinsed with ethanol. This procedure should result in only the grain boundaries being eroded away, revealing the crystal structure beneath.

An alternative etching with a mixture of 8 parts H_2O_2 to 1 part H_2SO_4c was also tested, but this eroded the crystal structure as well. It may be possible to use this as an etchant, though more testing to determine the etch duration would be necessary.

> After several trial runs, the final etching procedure was determined to consist of 10 to 20 seconds of swabbing a Q-tip soaked in etch solution on the sample, with a light pressure. Afterwards, the sample is first rinsed with water and then rinsed with ethanol. It is then dabbed dry on a Whatman lens cleaning tissue (to avoid scratching the surface). This yields a clean image with clearly distinct grain boundaries.

After etching, the samples are placed under a Zeiss Axioscope 7 microscope. The average grain size is determined using the ASTM E112-13 intercept method [32]. An example is also shown in figure 10. First, a composite photograph is taken at 50x magnification. On this photograph, a line is drawn. Intersections of crystal grain boundaries with this line are counted. The total length of the line is divided by the amount of intersections, and this gives an estimate for the crystal grain size. This is done four times for each pellet, at different heights (middle, 0.5 mm from edge, 1 mm from edge, 2 mm from edge).
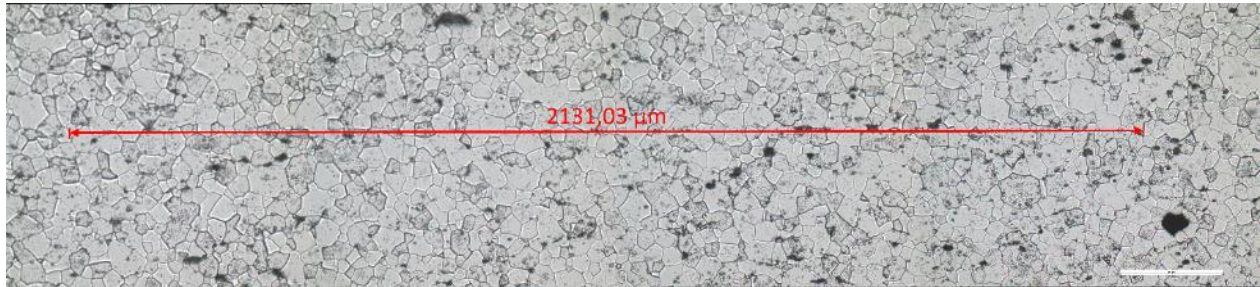

Figure 10: ASTM E112 intercept method example

4. Results and discussion

4.1 Characterization of starting materials

From the record of the pressure evolution in function of the gas volume provided to the sample (figure 11), the software on the device automatically provides an estimate for the specific surface of the samples. For the UO_2 reference sample, the software calculates a specific surface of 2.94 m²/g, while in reality it is 3.41 ± 0.04 m²/g. This under estimation by the BET analyser is known, but the technique is more used to compare the effect of different powder treatment procedures on the specific surface area of the powder. The software also calculates 2.39, 5.07 and 0.72 m²/g for the IDR UO_2 starting material, the Cr_2O_3 and the U_3O_8 respectively. A BET measurement of the ADU powder is not yet available
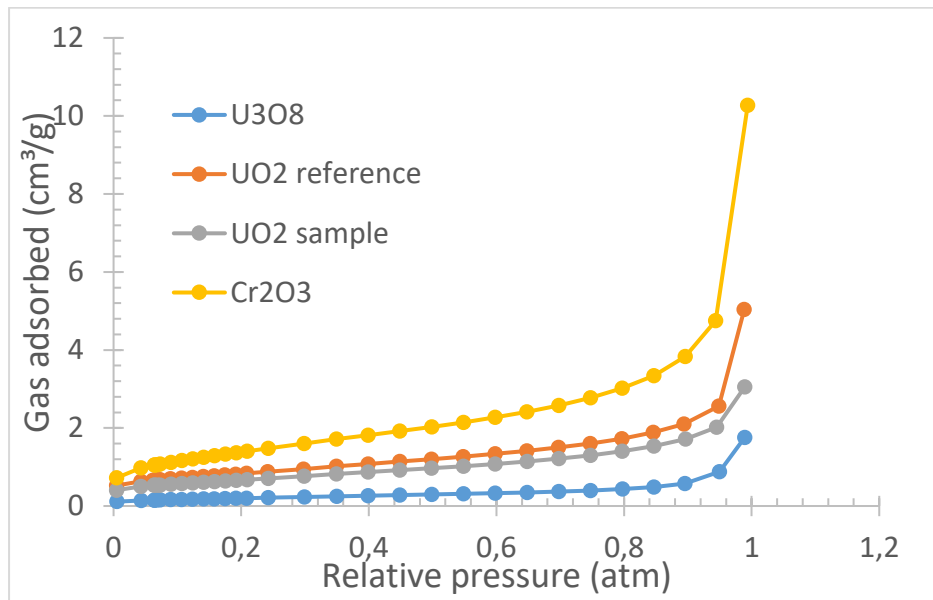

Figure 11: Isothermal adsorption graphs for the BET measurement

From the STA results, the O/U ratio of the UO_{2+x} starting powder can be determined. To obtain this ratio, the sample is first weighed. Then, it is oxidized in the STA. This turns all of the UO_2 present in the powder into U_3O_8, which has a fixed stoichiometry. As the molar mass of U_3O_8 is slightly higher than UO_2, the mass measured by the STA should slightly increase. From the final mass of the oxidized sample it is then possible to calculate the amount of UO_2 initially present in the powder. The STA graph is shown in figure 12. The measurement itself was part of a different project, but it concerns the same mother batch of powder and is fairly recent. Originally STA measurements on Cr_2O_3-doped pellets were also planned, but there were concerns that the chromium vapours released by this measurement could condense and damage other parts of the apparatus. There is a decrease present in the curve at the maximum temperature (900 °C). This decrease is due to the temporary formation of U_3O_{8-z}, a separate phase of uranium oxide that is not stable at room temperatures. For calculating the O/U ratio, the mass change at the 500 °C plateau is used, as there the stoichiometry of U_3O_8 is fixed.
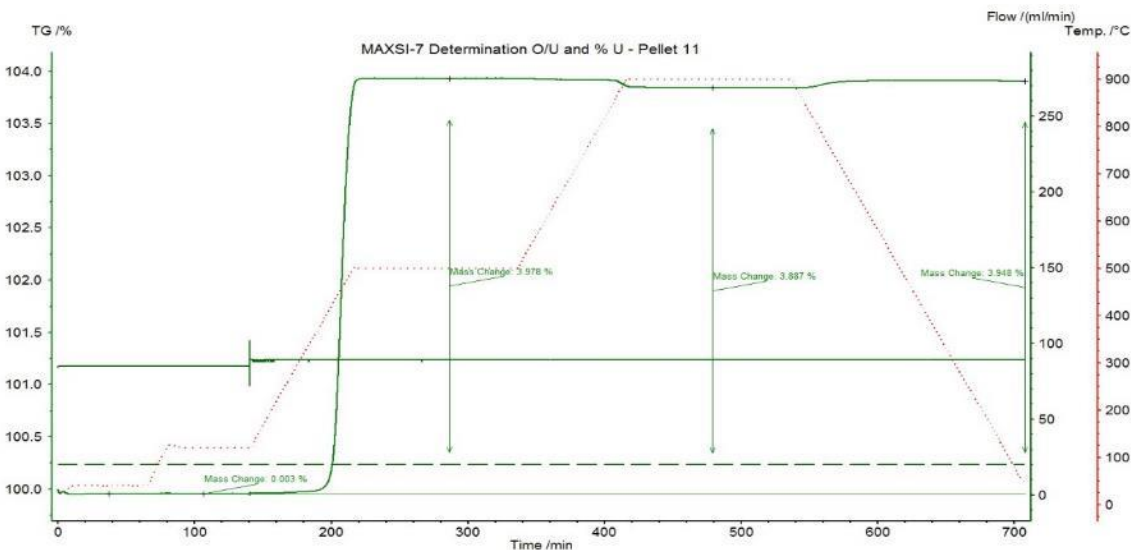
Figure 12: STA measurement of the IDR starting powder

In the case of oxidizing 3 UO_2 molecules to 1 U_3O_8 molecule, the mass increases by 3.95%. In this STA measurement, an increase of 3.978% was measured. Therefore, the UO_2 powder used was very slightly hypostoichiometric, with an O/U ratio of 1.996. This is only a basic way of determining the O/U ratio, as it does not take the oxidation of any impurities into account. As the powder is rather pure, it is not expected that the impurities present will impact the O/U ratio very much.

4.2 Visual inspection

Pellets were visually inspected for cracks and other defects. These were present in several of the IDR series (500, 600, 700, 900, 1000, 1100 ppm) due to a malfunction in their sintering. When these were first sintered, a blockage in the cooling flow of the furnace caused it to trip and shut down after reaching about 900 °C. Upon removing the fuel pellets from the furnace, they had darkened slightly. As these pellets were still below the temperature required for sintering to start, the entire cycle was restarted. Afterwards, it became clear something had definitely changed during that first sintering, as these pellets have considerably more defects (in particular radial and axial cracks) than other pellets.

In addition to this, some of the very first pellets produced during this study had pits on the surface. This was assumed to be because the starting powders used were not sieved before use. All subsequent batches were sieved and did not show these pits. Therefore it can be assumed that the pits are caused using unsieved powders. An explanation for the pits is that they may be formed when larger volumes of U_3O_8 powder clump together. These agglomerates then shrink more strongly as compared to the rest of the pellet matrix. They then come loose and fall out of the pellet as it shrinks further during sintering.

Another problem was identified during milling of the ADU batch. In an effort to reduce the particle size further than the IDR batch, this batch was first milled with the Turbula as usual, and then milled by hand in a pestle and mortar. As uranium dioxide can be pyrophoric when very finely divided, the milling by hand was performed under ethanol. During the drying, the wet UO_2 sludge was broken up and turned over to have it dry faster. It was then noticed that green spots (red circle in figure 13) were still present in the powder. These spots have the exact same appearance as Cr_2O_3. This gives reason to assume the

24

distribution of chromium(III) oxide in the finished pellets is not homogenous, but instead more clustered. If these pellets are to be produced for use in a reactor, a different milling device would be required to obtain homogeneity.

> The final pellet production procedure used was to first sieve(< 150 μm) all powders, then weigh and mix them to obtain the correct dopant levels and add 0.05 wt. % zinc stearate as press lubricant. This mixing was done in the Turbula, though it is recommended to find a more suitable mixing device for homogenous pellets. The powders are then pre-pressed at 2 to 4 kN (approx. 13-26 MPa), granulated to 20 mesh, rolled for 40 minutes, have 0.25 wt. % zinc stearate added and are rolled for an additional 12 minutes, before final pressing at 15 to 20 kN (approx. 99-130 MPa).

Figure 13: Image of inhomogeneities present in the ADU batch. Presumed to be Cr_2O_3.

4.3 Densities and effect of U_3O_8

Figure 14 shows the effect of the heating rate (slow and fast sintering) on immersion densities as more chromium(III) oxide is added. It is clear that a slow sintering produces more dense pellets overall. Figure 15 shows a comparison in density between pellets that had 10 wt.% UO_2 substituted for U_3O_8 and pellets that had 20 wt.% substitution for U_3O_8 before fast sintering. The reason the substitution was increased, was to obtain lower density pellets. 95-97 %TD is the desired target, and some pellets produced with 10 wt.% U_3O_8 are outside this range. During the sintering, U_3O_8 reduces to UO_2 and creates pores in the process. It is common practice to "recycle" UOX pellets by oxidizing them to U_3O_8 for use as pore former in a future batch. The targeted density range is also shown on figures 14 and 15.

For the 10 wt.% samples, it seems there is an almost linear increase in density with increasing amounts of chromium(III) oxide. However, for the 20 wt.% samples there seems to be no trend at all. Additionally,

all 20 wt.% samples are less dense than the 10 wt.% samples, illustrating the effect of U_3O_8 as a pore former.
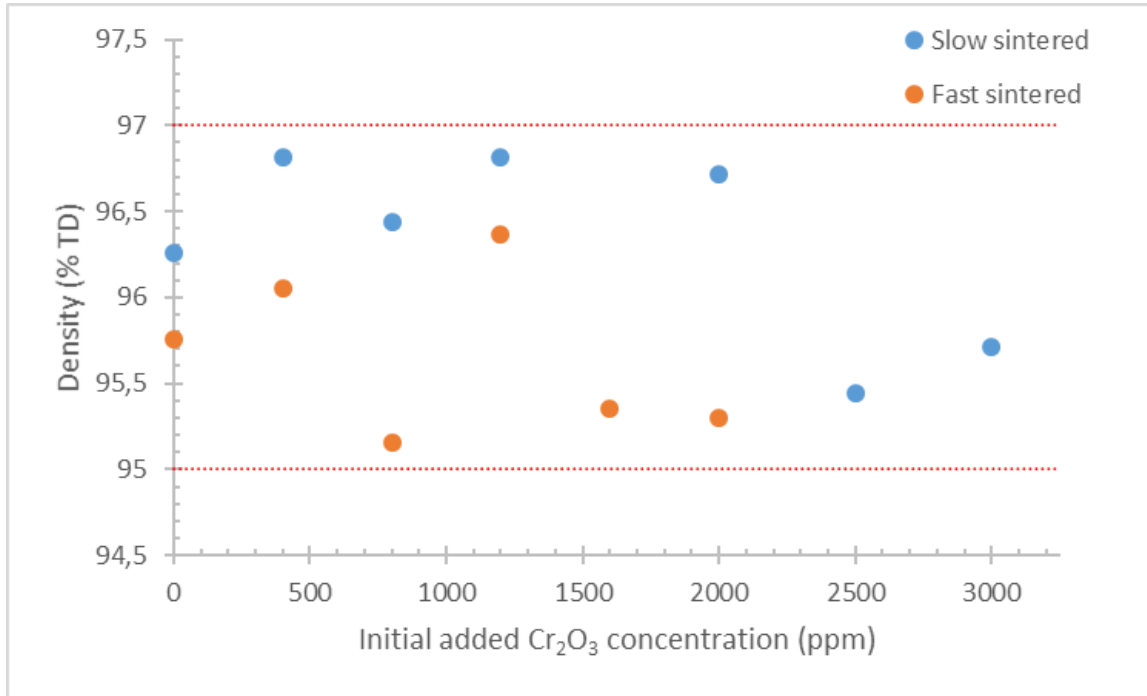

Figure 14: Densities resulting from fast sintering compared to densities from slow and fast sintering in 20 wt.% substituted powder
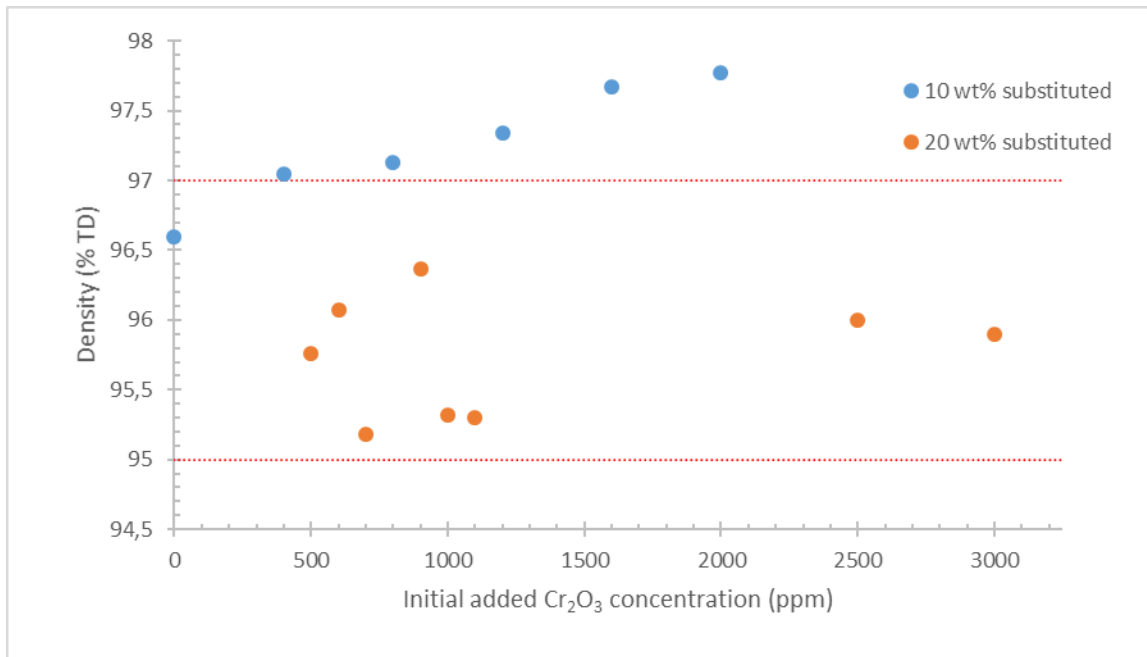

Figure 15: Density differences resulting from substituting UO_2 by U_3O_8 in fast-sintered powder

4.4 Etching and average crystal grain size

After examination of several iterations of the etching procedure, it was concluded that submerging the pellet surface is not a reproducible way of etching the surface. Some pellets had clear crystal structures visible after being submerged for 20 seconds, while others were still hidden after 90 seconds. Etching too long also causes the crystal structures to discolour, which makes it hard to accurately determine the grain size. The discoloration may be caused by the embedding resin being attacked by the etchant.

A few attempts were made to use the piranha etch instead, but this etch resulted in the crystal grains being damaged beyond boundaries identification (figure 16). The surface is so uneven after the piranha etch that the microscope cannot achieve a proper focus across the entire screen. During the etching experiments a different microscope was used closer to the lab, to be able to compare the effect of different etching conditions more quickly.

Figure 16: Damage resulting from the piranha etch

After testing several iterations of the etching, the etch procedure used at FBFC was re-examined. This one also included 30 seconds of "rubbing" the sample with a cotton swab soaked in the etch solution, which was initially replaced with 10 additional seconds of submersion. However, after swabbing a previously etched (and discoloured) sample with a Q-tip soaked in etchant, the discoloration disappeared and the samples appeared to have been etched quite evenly. Even for fresh samples, swabbing for 10-20 seconds (without submersion) at moderate pressure is enough to fully reveal the crystal grains. Figure 17 shows an example of a successfully etched surface.

> After several trial runs, the final etching procedure was determined to consist of 10 to 20 seconds of swabbing a cotton Q-tip soaked in etch solution on the sample, with a light pressure. Afterwards, the sample is first rinsed with water and then rinsed with ethanol. It is then dabbed dry on a Whatman lens cleaning tissue (to avoid scratching the surface). This yields a clean image with clearly distinct grain boundaries.
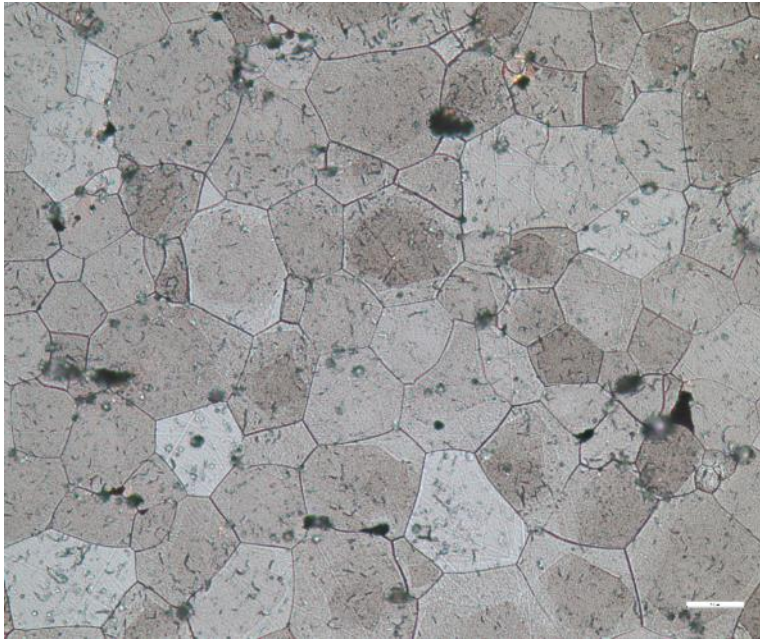
Figure 17: Revealed crystal grain boundaries after etching

The same Q-tip cannot be used for multiple pellets in a row, as the etch composition quickly seems to degrade and turn from orange to green. Once it has turned green, it is no longer able to etch the pellets. This degradation seems to be due to the cotton present in the Q-tip, as a poured solution of etchant (e.g. on a watch glass) stays orange and turns brown as it evaporates. In addition to this, storing the etch solution for 2 days or more causes it to lose its etching capabilities, even when it is stored in a sealed bottle. If it degrades this way, it stays orange in colour.

Figure 18 shows a pellet (IDR batch, with 800 ppm Cr_2O_3) from the etching tests. Dark and clear areas can clearly be seen on the pellet surface. The dark areas have much smaller crystals than the clear areas. This could be explained with the heterogeneous distribution of chromium which had already been seen to not properly mix in the ADU mixture. In addition, EPMA measurements confirm that chromium(III) is spread inhomogenously throughout the 1000 and 1100 Cr_2O_3 ppm IDR pellets. It is therefore assumed that the chromium(III) oxide in the rest of the IDR batch is also heterogeneous, and it is possible that large-crystal areas are only formed around agglomerates of chromium(III) oxide. This would mean that the grain sizes obtained in this study are an underestimation, as the ASTM E112 intercept method would also take small (low-doped of undoped regions) grains into account. A completely homogenous chromium(III) oxide-doped pellet would then have an increased grain size across the entire surface, which would lead to a higher reported average grain size. The grain sizes obtained are tabulated below, in table 3, and shown side by side with data from other studies in figure 19.

From the data presented here, it can be seen that grain size increases up to 600 ppm Cr_2O_3. After that, there is a slight decrease in crystal grain size. This decrease is also present in other studies and is generally attributed to the limit of solubility of Cr_2O_3 in UO_2, approximately 650 ppm [10]. However, in our case, the decrease appears at a lower Cr_2O_3 concentration when compared to other studies. The second peak around 2500 ppm Cr_2O_3 present in other studies is not very pronounced in our results, if it is even there. We also do not reach grain sizes close to Bourgeois' results (33 µm versus 86 µm), or even close to results from Jaan Teelen's study [33] (listed as Wet coating) at the SCK (a maximum 62

28

μm). This is a clear indication that wet coating is superior technique compared to dry mixing in terms of resulting crystal grain size, as the equipment and starting powders should be identical in this study and Teelen's. Additionally, co-precipitation seems to perform worst of all when considering the resulting crystal grain size.

More crystal grain size measurements are planned and may be found in a later publication. These include grain sizes of ADU-based pellets (both fast and slow sintered) and slow sintered IDR pellets. The pellets themselves were produced, but not yet ready for etching at the time of writing.
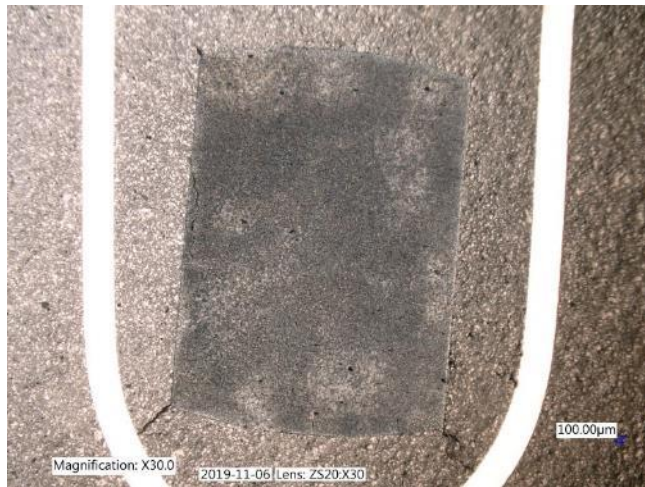

Figure 18: Pellet overview of one of the etching samples, showing inhomogeneous crystal growth

Table 3: Average grain size with regard to Cr_2O_3 dopant level, IDR batch (fast sintering only)

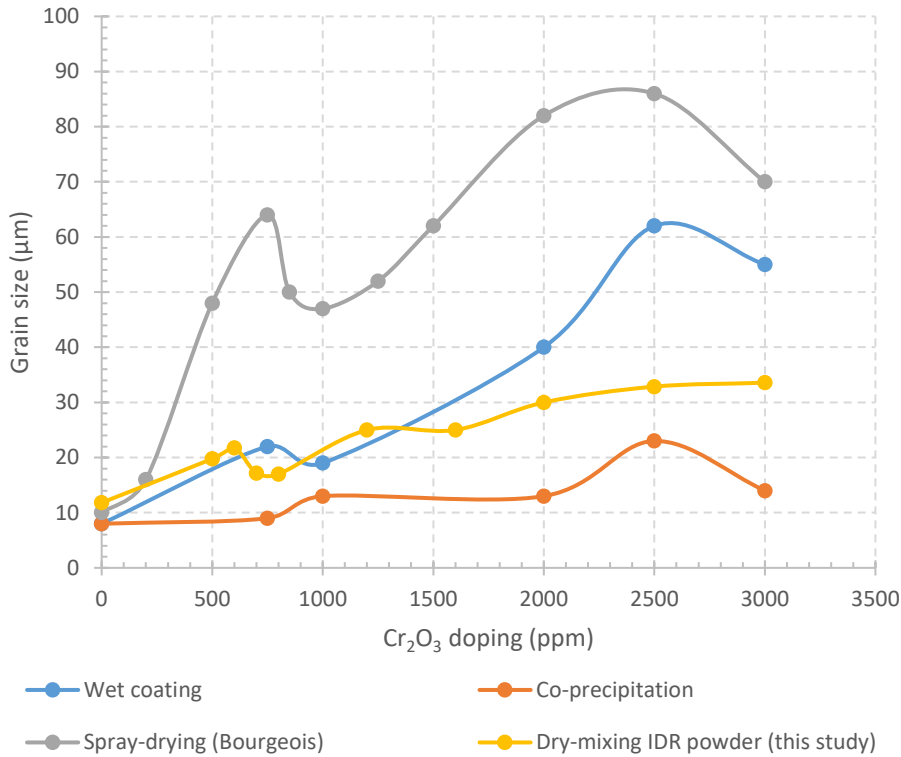| Dopant level (ppm)	Average grain size (μm)
0	11.8
400	11.8
500	19.8
600	21.7
700	17.2
800	17
1200	25
1600	25
2000	30
2500	32.9
3000	33.6

Figure 19: Grain growth in function of dopant level for several studies. Wet-coating and Co-precipitation [33] *data points are from in-house studies at the SCK, which have not been published.*

4.5 Dilatometry

As stated in par. 2.1.4.4, dilatometry was performed for 9 IDR samples with dopant levels varying between 0 and 3000 ppm Cr_2O_3. The changes in length reported by the dilatometer were transformed to changes in density by assuming the pellet shrink is more or less equal both axially and radially. Then, the density before and after dilatometry were used to fit the data profile. This yields the graphs in figure 20. This data can be combined with the dL/dt reported by the dilatometer to obtain dρ/dt, the rate of densification. This is shown in figure 21. For these graphs, only the heating and holding time have been plotted (the holding time results in a straight vertical line, as the sample is kept at a constant temperature). The cooling segment has been removed as the sintering process is assumed to be fully completed after the holding time.
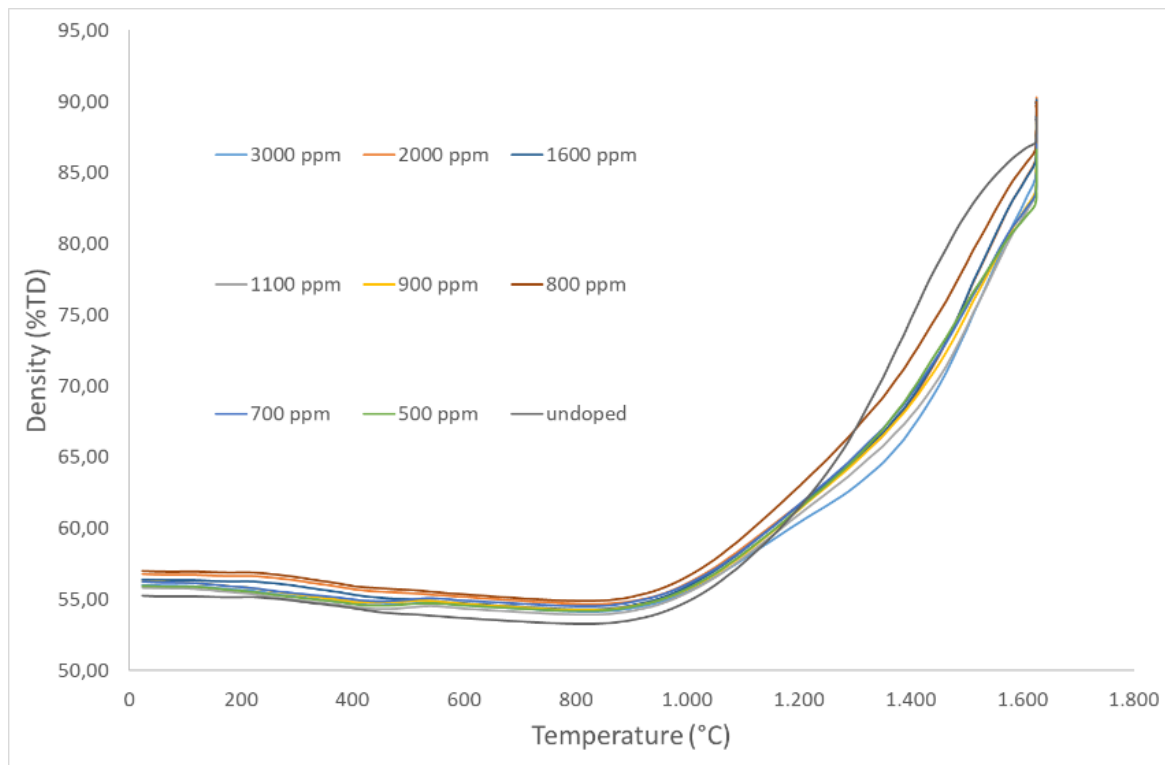
Figure 20: Evolution of density for sintering of chromia-doped uranium pellets
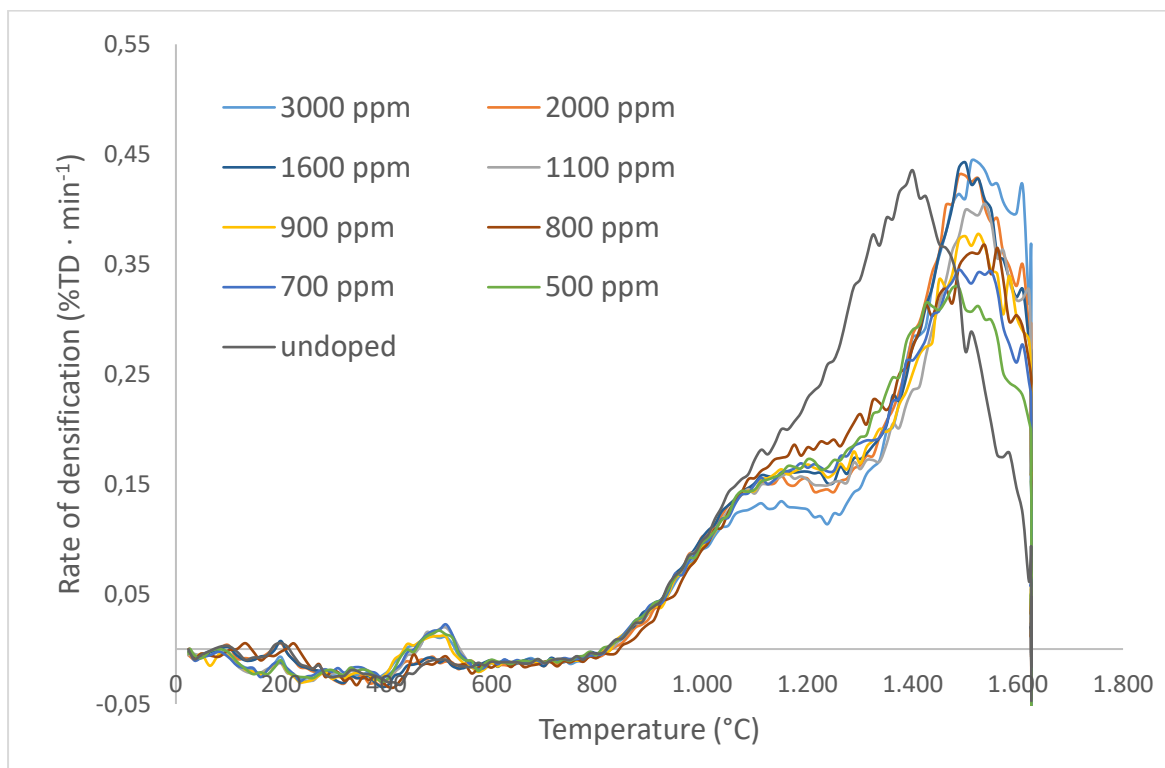

Figure 21: Plot of rate of densification for sintering of chromia-doped uranium pellets

From the graphs it can be seen undoped pellets reach a maximum densification rate at a lower temperature compared to chromia-doped pellets. The addition of chromium(III) oixde shifts the peak in sintering speed upwards by about 200 degrees, regardless of chromium(III) oxide content. However, the chromium(III) oxide content does affect the actual sintering speed, with higher concentrations of chromium(III) oxide initially hindering the sintering: on figure 20 it can be clearly seen that sintering speed plateaus between temperatures in the 1000-1300 °C range for chromia-doped pellets. The higher the chromium(III) oxide content, the lower this plateau. After the plateau phase, the rate of densification increases again to a maximum, with more chromium(III) oxide leading to a higher maximum densification rate. The three highest dopant levels (1600, 2000 and 3000) reach approximately the same maximum rate, which is slightly higher than undoped uranium oxide.

The crystal size-enhancing effect of chromium(III) is usually attributed to two phenomena. First is the formation of a Cr-O liquid eutectic by the chromium and second is an increased amount of vacancies present in the uranium. These vacancies improve uranium mobility during sintering. The eutectic only forms at temperatures above about 1650 °C, which is not reached during these dilatometry experiments. Therefore, the effects of chromium(III) oxide on grain growth during sintering seen in this study are likely only due to the vacancy effect. More specifically, chromium(III) oxide seems to initially suppress grain growth at lower temperatures (1000-1300 °C), while enhancing it at higher temperatures (1400-1600 °C), based on this data.

This behaviour can be mostly explained by findings from the literature study. The addition of chromium(III) oxide beyond the limit of solubility creates a second, solid phase in the pellets. This phase suppresses sintering by pinning grain boundaries, causing the plateau at 1000-1300 °C. Theoretically, this should not affect the 500 and 700 ppm samples, as these are still below the limit of solubility of Cr_2O_3 in UO_2. However, even at concentrations below the limit of solubility, chromium(III) oxide can form precipitates in some areas, which will inhibit sintering. As the temperature increases, the chromium(III) oxide causes more uranium vacancies to form as shown in Cooper's [29] simulations. These vacancies improve uranium mobility, thus increasing the sintering speed and compensating for the effect of the second solid phase.

Further research could include a dilatometric study with even higher temperatures, as this study does not have data regarding the Cr-O eutectic. Including slower heating rates in the dilatometry would also be interesting, as Bourgeois [7] shows that the heating rate severely impacts the sintering kinetics in his thesis [6], though he does not mention it in his paper.

4.6 XRD

A sample spectrum is shown in figure 22. Here, the red spectrum corresponds to the measurement, while the blue one corresponds to a reference sample of pure UO_2. Again, as there was no monochromator available for these measurements, all peaks are twinned due to the Cu $K_{\alpha2}$ reflections also being present. For most peaks the software automatically identifies these and excludes these from calculations. Where the software was not able to automatically remove them, they were excluded by hand.

Table 4 shows all the XRD results, together with Vegard's law [34]. Vegard's law is an empirical formula to somewhat predict the crystal lattice parameter resulting from a mixture of two solids "A" and "B" on the condition that they have the same crystal structure. It can be expressed as follows:

$$a_{comp} = x\, a_A + (1 - x)a_B \tag{3.1}$$

Where a refers to the lattice parameter and x refers to the mass fraction of the composite material comprised of solid "A". For pure UO_2 a was taken to be equal to 547.115 pm, and for pure Cr_2O_3 a was taken to be equal to 495 pm.

Error bars were calculated using propagation of errors, using formula (3.2) below

$$\sigma = \sqrt{\sum \sigma_i{}^2} \tag{3.2}$$

Here, σ represents the total uncertainty on the measurement, while σ_i are individual uncertainties (e.g. due to temperature effects, error inherent to the XRD apparatus, uncertainty on the wavelength and uncertainty introduced by the analysis software). Of these, the uncertainties related to temperature and the apparatus were dominant in the calculation, making the error bars nearly constant.
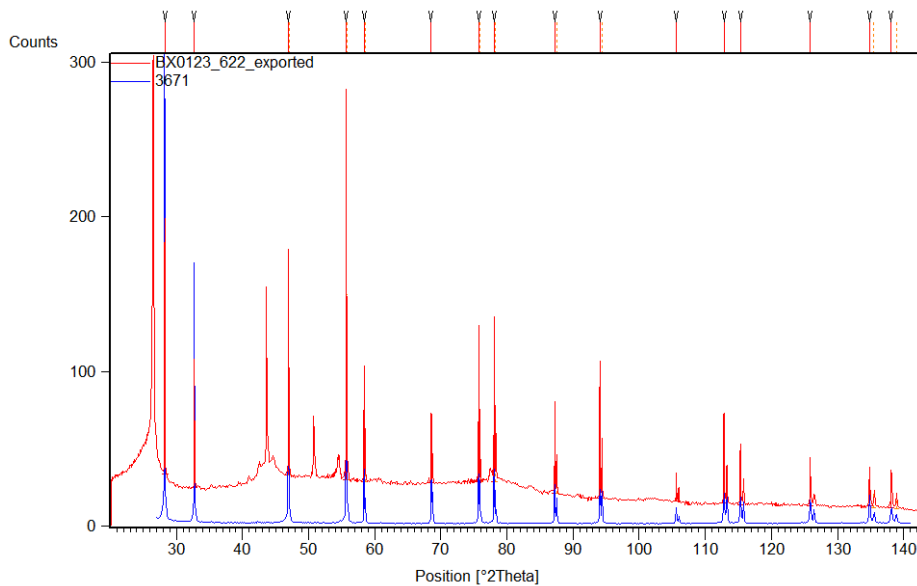

Figure 22: Sample XRD spectrum. Red: test sample, Blue: UO₂ reference. Arrows at the top indicate peaks considered for reference cell determination.

| Initial Cr$_2$O$_3$ content (ppm)	Lattice parameter (Ä)	Snyder FOM	Vegard's law
0	5.47115	800.87	5.47115
400	5.47076	635.42	5.47094
500	5.47091	354.94	5.47089
600	5.47102	531.37	5.47084
700	5.47050	61.73	5.47079
800	5.47067	361.71	5.47073
900	5.47077	354.25	5.47068
1000	5.47075	465.56	5.47063
1100	5.47089	524.77	5.47058
1200	5.47053	353.81	5.47052
1600	5.47028	396.01	5.47032
2000	5.47028	494.18	5.47011
2500	5.47023	560.30	5.46985
3000	5.47014	399.58	5.46959
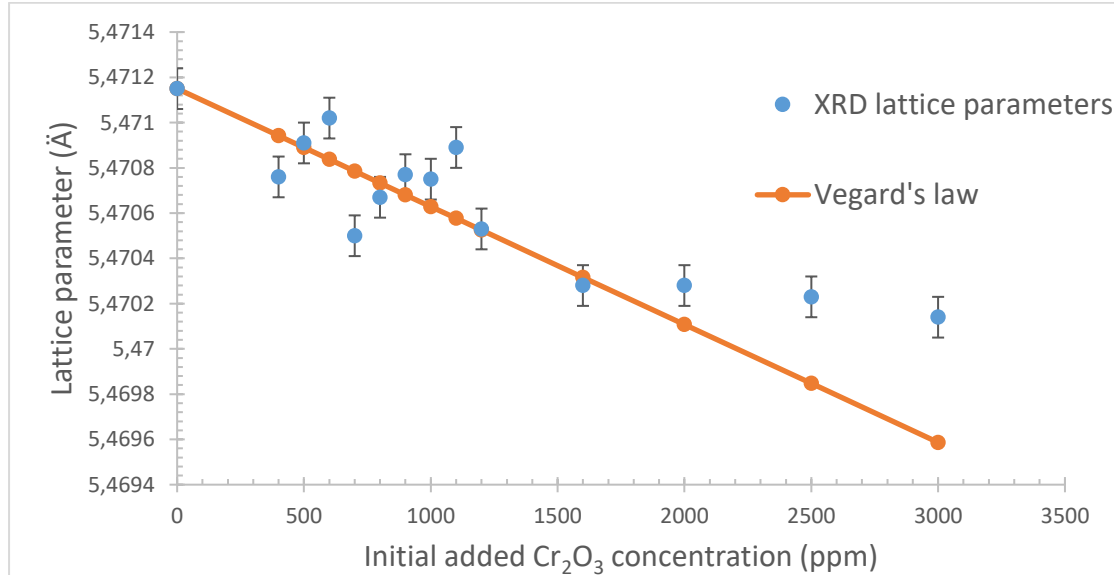
Figure 23: XRD results of fast sintered IDR pellets, together with lattice parameters predicted by Vegard's law [34]

From the XRD results it follows that, as more chromium(III) oxide is added, overall the crystal lattice contracts. This contraction continues up to a certain point (about 1200-1600 ppm Cr$_2$O$_3$), after which the crystal lattice stays more or less the same. Cardinaels et al. [8] concluded that Cr(III) will either substitute for U atoms in the crystal lattice or cause O vacancies to appear, both of which cause the lattice to contract overall, based on similar measurements. They concluded this by examining the energies

34

associated with the creation of crystal defects in UO_2. Those two effects are energetically favorable compared to other means of incorporating Cr(III).

There is a large spread on measured lattice constants, especially at lower Cr_2O_3 concentrations. This is due some Cr_2O_3 evaporating during sintering and possible inaccuracies during the weighing of Cr_2O_3. This, however, does not explain points below the Vegard's law curve, as evaporation of Cr_2O_3 should shift points to the left, not down.

From our data it appears that there is a limit to the uptake of Cr_2O_3, as the lattice constant plateaus. This would mean that either the Cr_2O_3 is not incorporated at all in this plateau. This saturation behaviour is caused by the limit of solubility. The reason this seems to occur at a higher chromium(III) oxide concentration (1600 compared to 700 ppm), is due to the loss of chromium(III) during sintering.

4.7 EPMA

Figure 24 shows the result of the line scan. It shows chromium(III) is not dispersed homogenously, reaching concentrations of over 1200 ppm in one particular region of the pellet, which only had 1000 ppm Cr_2O_3 added initially.

The average chromium content across the line scan for pellet 1 was 553 ppm Cr(III), which translates to 813 ppm Cr_2O_3. Therefore, about 19% of the added Cr_2O_3 evaporated during sintering. Pellet 2 had an average of 456 ppm Cr(III), translating to 670 ppm Cr_2O_3. As the initial concentration of Cr_2O_3 in this pellet was 1100 ppm, about 31% of the added Cr_2O_3 evaporated during sintering.

Figure 25 shows a heat map of the chromium(III) distribution in pellet 1. It was reconstructed from the mapping data. This mapping produced three separate 1024x800 plots, which were each transformed into a heat map using Python and then stitched together to form figure 25. Yellow tones correspond to high Cr(III) concentrations, while blue tones correspond to low Cr(III) concentrations. Important of note in this picture is the difference between the rightmost and leftmost sides, with the right side having a higher concentration of Cr(III), as can also be seen in the line scan. There seems to be a slight discontinuity between the centre and rightmost maps. There may have been some data points in between that did not get measured.
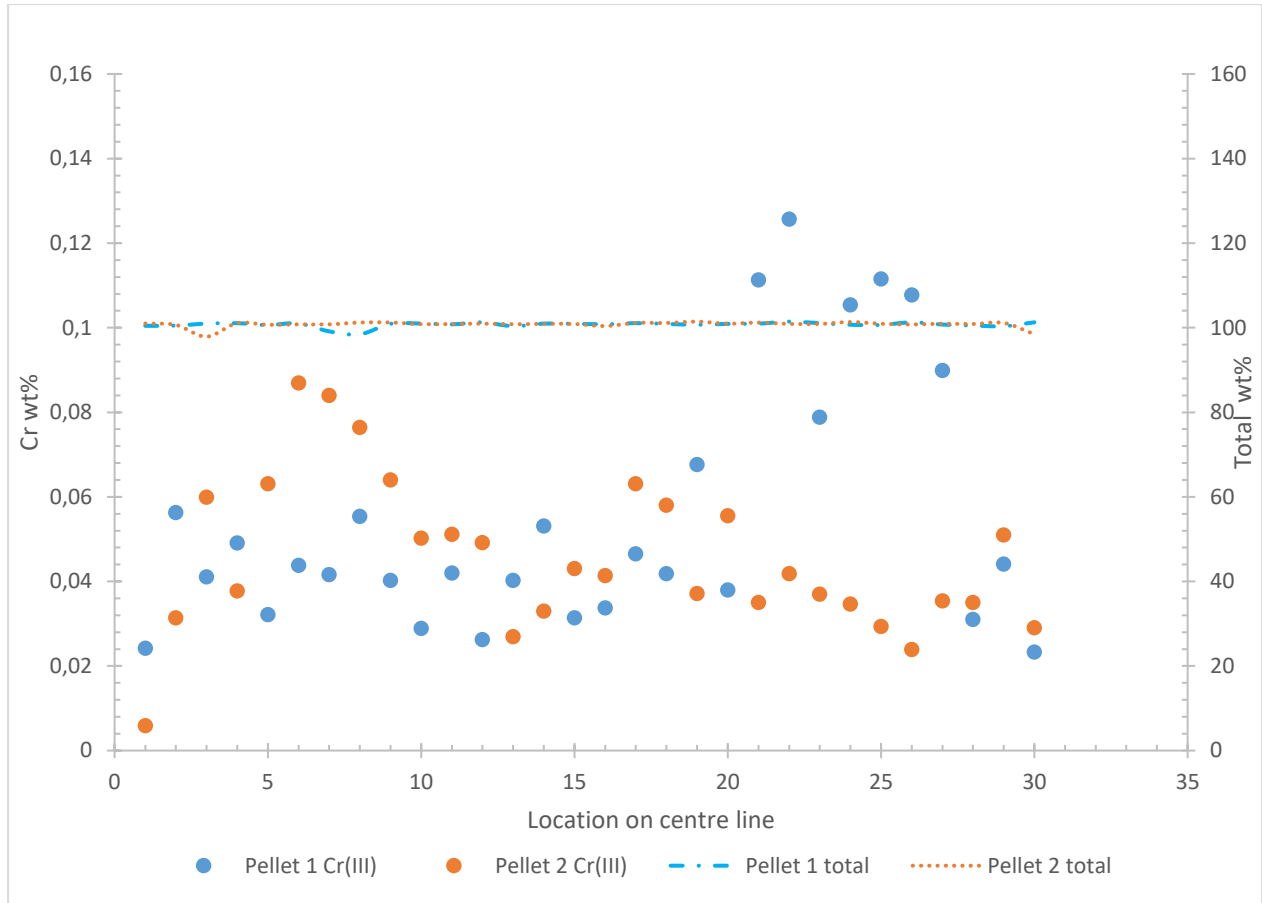
Figure 24: Result of the EPMA line scan. Pellet 1 initially contained 1000 ppm Cr_2O_3, pellet 2 contained 1100 ppm Cr_2O_3.
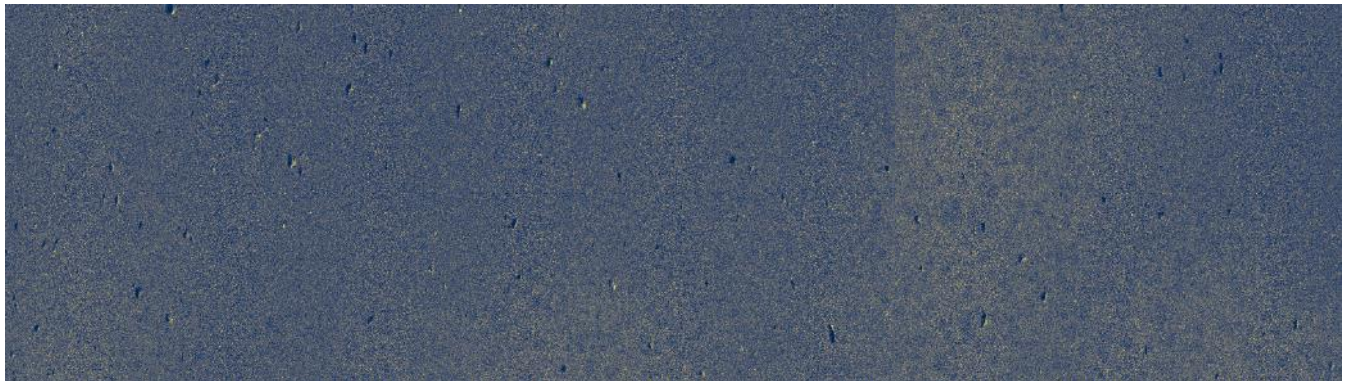

Figure 25: Coloured heatmap of the "mapping mode" EPMA measurement on the 1000 ppm Cr_2O_3 pellet (pellet 1 in fig. 24)

36

5. Conclusion

5.1 Effects of chromium(III) oxide doping

The addition of chromium(III) oxide does increase the crystal grain size of fuel pellets. Increased average crystal grain sizes were observed across all chromium(III) dopant levels, but the areas of increased crystal growth were inhomogenously scattered throughout the pellets. EPMA confirmed that there are areas which have a higher chromium(III) content. Although the data in this study cannot definitively prove that areas with a higher chromium(III) content are those with enlarged grains, it is rather probable that the inhomogenous spread of chromium(III) lead to inhomogenous crystal growth. In this study, the chromia-doped, dry mixed IDR-based pellets reach a maximum average grain size of 33 µm, which is about a 200% increase when compared to similar, undoped pellets which are typically in the range between 8 to 12 µm.

5.2 Inhomogeneity

Based on the presence of Cr_2O_3 agglomerates after milling, both seen visually and in the inhomogenous crystal grain size distribution, the Turbula is not suited to produce homogenous pellets with these starting powders by dry mixing and milling. Either a different milling device, a different way of doping or a finer batch of Cr_2O_3 powder is required. Other ways of adding the Cr_2O_3 powder, like wet coating [33] or spray coating [6], seem to perform better in terms of increasing the grain size. Another technique, co-precipitation, seems to be the only technique to perform worse than dry milling. It should be noted that Bourgeois' chromium(III) oxide powder may have been more fine and that this may have impacted his results.

5.3 XRD

XRD confirms that the chromium(III) oxide is at least partially integrated into the fuel matrix. During this integration, the overall crystal slightly contracts. This integration plateaus around 1600 ppm initially added. During sintering, a part of the chromium(III) oxide will become volatile and thus the actual concentration present in the pellet afterwards is lower. Therefore, the initial 1600 ppm may correspond to the limit of solubility of chromium(III) in UO_2, which is about 650 ppm [10]. Any excess chromium(III) present precipitates out and forms metallic depositions inside the fuel pellets. These depositions do not contribute to grain growth, hindering it instead.

5.4 Kinetics

Adding chromium(III) oxide influences the behaviour of chromium-doped pellets during sintering. For all concentrations of chromium(III) oxide, the sintering rate decreases as compared to undoped UO2 in the temperature range of 1000-1400 °C. In fact, it is as if the chromium(III) oxide causes the sintering rate graph to shift about 200 °C upwards. This may be caused by the chromium(III) oxide pinning the grain boundaries, which hinders the initial stages of sintering. Thus, when the sample is being heated, it will spend more time in the first and second stage of sintering. This may be responsible for enlarged grains in the final pellets as compared to undoped pellets.

From the data available it seems that in terms of resulting grain size wet coating is superior to dry milling, which in turn is superior to co-precipitation.

5.5 Outlook

Future research should include a more in-depth determination of the crystal grain size for ADU pellets, which should, ideally, have varied sintering profiles. A characterization of ADU UO_2 would also be interesting.

Analyzing samples with dilatometry with a slow sintering may also lead to interesting results. In addition, raising the maximum sintering and dilatometry temperature from 1625 °C to 1700 °C might result in another sharp increase in crystal grain size, as at those temperatures the Cr-O eutectic should form, where in this study only the vacancy effect was present.

This study could also be repeated for wet coated, co-precipitated or other forms of doped uranium. It would be interesting to have a complete data set on each of these (both slow and fast sintered), to be able to compare doping techniques. A complete view of all doping procedures and sintering conditions would allow for optimization of the production of doped pellets.

6. References

[1]   C. Rivollier, P. Fauvel, and P. Heisch, "Fuel of the future," *Hydrocarb. Eng.*, vol. 13, no. SUPPL. AUTUMN, 2008.

[2]   Framatome, "Framatome's EATF Program." [Online]. Available: https://nextevolutionfuel.com/framatome-eatf-program/. [Accessed: 15-Dec-2019].

[3]   European Commission, "Home - Modern Spent Fuel Dissolution and Chemistry in Failed Container Conditions." [Online]. Available: https://www.disco-h2020.eu/. [Accessed: 03-Oct-2019].

[4]   J. C. Killeen, "Fission gas release and swelling in UO2 doped with Cr2O3," *J. Nucl. Mater.*, vol. 88, no. 2–3, pp. 177–184, 1980.

[5]   S. Kashibe and K. Une, "Effect of additives (Cr2O3, A12O3, SiO2, MgO) on diffusional release of 133Xe from UO2 fuels," *J. Nucl. Mater.*, vol. 254, no. 2–3, pp. 234–242, 1998.

[6]   L. Bourgeois, "Contribution a l'etude du role de dopants dans la densification et la croissance cristalline du dioxyde d'uranium," Centre d'Etudes Nucléaires de Grenoble, 1993.

[7]   L. Bourgeois, P. Dehaudt, C. Lemaignan, and A. Hammou, "Factors governing microstructure development of Cr2O3-doped UO2 during sintering," *J. Nucl. Mater.*, vol. 297, no. 3, pp. 313–326, 2001.

[8]   T. Cardinaels *et al.*, "Chromia doped UO 2 fuel: Investigation of the lattice parameter," *J. Nucl. Mater.*, vol. 424, no. 1–3, pp. 252–260, 2012.

[9]   C. Riglet-Martial *et al.*, "Thermodynamics of chromium in UO2 fuel: A solubility model," *J. Nucl. Mater.*, vol. 447, no. 1–3, pp. 63–72, 2014.

[10] A. Leenaers, L. De Tollenaere, C. Delafoy, and S. Van den Berghe, "On the solubility of chromium sesquioxide in uranium dioxide fuel," *J. Nucl. Mater.*, vol. 317, no. 1, pp. 62–68, 2003.

[11] T. Allen, J. Busby, M. Meyer, and D. Petti, "Materials challenges for nuclear systems," *Mater. Today*, vol. 13, no. 12, pp. 14–23, 2010.

[12] B. Cox, "Pellet-clad interaction (PCI) failures of zirconium alloy fuel cladding - A review," *J. Nucl. Mater.*, vol. 172, no. 3, pp. 249–292, 1990.

[13] T. Alam, M. K. Khan, M. Pathak, K. Ravi, R. Singh, and S. K. Gupta, "A review on the clad failure studies," *Nucl. Eng. Des.*, vol. 241, no. 9, pp. 3658–3677, 2011.

[14] C. S.-C. D. Leboulch, L. Fournier, "Testing and Modelling Iodine-induced Stress Corrosion Cracking in Stress-relieved Zircaloy-4," in *Pellet-clad Interaction in Water Reactor Fuels*, 2005, no. March, pp. 367–377.

[15] A. L. Lowe and G. W. Perry, "Zirconium in the Nuclear Industry: 3rd Conference - STP 633," in *Proc. 3rd Int. Conf. on Zirconium in the Nuclear Industry*, 1976, p. 281.

[16] J. H. Schemel, "Zirconium in the Nuclear Industry: 4th Conference," 1978, p. 145.

[17] J. Arborelius *et al.*, "Advanced doped UO 2 pellets in LWR applications," *J. Nucl. Sci. Technol.*, vol. 43, no. 9, pp. 967–976, 2006.

[18] S. E. Ion and R. H. Watson, "20 Years of Production of UO2 by the Integrated Dry Route–A BNFL

Perspective on Dry Conversion," *A Collect. Pap. Eng. Asp. Fabr. Ceram. Ceram. Eng. Sci. Proceedings, Vol. 14, Issue 11/12*, vol. 154, no. 1993, pp. 149–154, 2008.

[19]   I. A. E. Agency, "Nuclear Fuel Cycle Information System - A Directory of Nuclear Fuel Cycle Facilities 2009 Edition," *Iaea, Vienna, 2009*, no. April, 2009.

[20]   L. F. Francis, "Materials processing," in *Materials Processing*, 1st editio., Elsevier, 2016, pp. 343–414.

[21]   A. R. Khoei, "Powder Constitutive Models," *Comput. Plast. Powder Form. Process.*, pp. 44–100, 2005.

[22]   J. Vleugels, *KuLeuven Course material: Ceramics and powder metallurgy*. 2019.

[23]   M. N. Rahaman, *Ceramic processing and sintering*, Second edi. New York: CRC Press.

[24]   M. Prakasam, J. Locs, K. Salma-Ancane, D. Loca, A. Largeteau, and L. Berzina-Cimdina, "Fabrication, Properties and Applications of Dense Hydroxyapatite: A Review," *J. Funct. Biomater.*, vol. 6, no. 4, pp. 1099–1140, 2015.

[25]   V. J. Wheeler and I. G. Jones, "Thermodynamic and composition changes in UO2±x (x< 0.005) at 1950 K," *J. Nucl. Mater.*, vol. 42, no. 2, pp. 117–121, 1972.

[26]   J. Arborelius *et al.*, "Advanced doped UO 2 pellets in LWR applications," *J. Nucl. Sci. Technol.*, vol. 43, no. 9, pp. 967–976, 2006.

[27]   V. Peres *et al.*, "High temperature chromium volatilization from Cr2O3 powder and Cr2O3-doped UO2 pellets in reducing atmospheres," *J. Nucl. Mater.*, vol. 423, no. 1–3, pp. 93–101, 2012.

[28]   C. Mieszczynski *et al.*, "Microbeam x-ray absorption spectroscopy study of chromium in large-grain uranium dioxide fuel," *J. Phys. Condens. Matter*, vol. 26, no. 35, 2014.

[29]   M. W. D. Cooper, C. R. Stanek, and D. A. Andersson, "The role of dopant charge state on defect chemistry and grain growth of doped UO2," *Acta Mater.*, vol. 150, pp. 403–413, 2018.

[30]   N. Y. Toker, L. S. Darken, and A. Muan, "Equilibrium phase relations and thermodynamics of the Cr-0 system in the temperature range of 1500 °C to 1825 °C," *Metall. Trans. B*, vol. 22, no. 2, pp. 225–232, 1991.

[31]   H. Kleykamp, "Phase equilibria in the UO2-austenitic steel system up to 3000°C," *Nucl. Mater.*, vol. 247, pp. 1–224, 2011.

[32]   ASTM international, "ASTM E112-13, Standard Test Methods for Determining Average Grain Size." West-Conshohoken, PA, 2013.

[33]   J. Teelen, "Unpublished thesis," UHasselt, 2019.

[34]   L. Vegard, "Die konstitution der mischkristalle und die raumfüllung der atome," *Zeitschrift für Phys. A Hadron. Nucl.*, 1921.

7. Appendix

A. Details of the IDR powder used in this study

AREVA

FBFC-LABORATOIRE
ROMANS sur ISERE

PROCES-VERBAL DE CONTROLE

Numéro: 186507 **Révision:** 0

LAB - F - 75 Rév.9
Logiciel L511420
Tél. 04 75 05 60 00
Poste 6319

Impuretés

Al	<	12		µg/g UO2	BTN	Conforme	BMY	511229	
B	<	0.28		µg/g UO2	BTN	Conforme	BMY	511229	
Bi	<	1		µg/g UO2	BTN	Conforme	BMY	511229	
C	=	26	+-3	µg/g UO2	CBN	Conforme	ART	511165	
Ca	=	11	+-4	µg/g UO2	BTN	Conforme	BMY	511230	
Cd	<	0.4		µg/g UO2	BTN	Conforme	BMY	511229	
Cl	<	4		µg/g UO2	CDR	Conforme	MNY	511121	
Co	<	2		µg/g UO2	BTN	Conforme	BMY	511229	
Cr	=	6.2	+-5.2	µg/g UO2	BTN	Conforme	BMY	511229	
Cu	<	3		µg/g UO2	BTN	Conforme	BMY	511229	
F	=	15.4	+-2.3	µg/g UO2	MNY	Conforme	ART	511069	
Fe	=	12	+-7	µg/g UO2	BTN	Conforme	BMY	511229	
In	<	4		µg/g UO2	BTN	Conforme	BMY	511246	
Mg	<	5		µg/g UO2	BTN	Conforme	BMY	511229	
Mn	<	3		µg/g UO2	BTN	Conforme	BMY	511229	
Mo	<	16		µg/g UO2	BTN	Conforme	BMY	511229	
N	<	8		µg/g UO2	CDR	Conforme	MNY	511118	
Pb	<	3		µg/g UO2	BTN	Conforme	BMY	511229	
Ni	<	12		µg/g UO2	BTN	Conforme	BMY	511229	
Si	<	20		ug/g UO2	BTN	Conforme	BMY	511229	
Sn	<	4		µg/g UO2	BTN	Conforme	BMY	511229	
Th	<	2		µg/g UO2	MDS	Conforme	BMY	511231	
Ti	<	5		µg/g UO2	BTN	Conforme	BMY	511229	
V	<	1		µg/g UO2	BTN	Conforme	BMY	511229	
W	<	12		µg/g UO2	BTN	Conforme	BMY	511235	
Zn	<	10		µg/g UO2	BTN	Conforme	BMY	511229	

Isotopie

U234	=	0.001	+- 0.001	g/100g U	BMY		MLC	511295	
U235	=	0.319	+- 0.007	g/100g U	BMY	Non conforme	MLC	511295	CA: U235 = 0.320+-0.007 g/100gU
U236	<	0.002		g/100g U	BMY		MLC	511295	
U238	=	99.680	+- 0.010	g/100g U	BMY		MLC	511295	
U234/U235	=	3135		µg/g	BMY	Conforme	MLC		
U236/U235	=	6270		µg/g	BMY	Conforme	MLC		

Rapport stoechiométrique

O/U	=	2.06	+-0.01	at/at	BTN	Conforme	BMY	511045	

Tamisage

Tam 400 µm	=	10.00		Refus Tamis	GRT		CIT	
Tam 710 µm	=	0		Refus Tamis	GRT	Conforme	CIT	

Teneur en humidité

H2O	=	0.09	+-0.02	g/100g UO2	ART	Conforme	MNY	511027

Teneur en Uranium

U	=	87.75	+-0.04	g/100g UO2	BTN	Conforme	BMY	511045

PROCES-VERBAL DE CONTROLE

AREVA

FBFC-LABORATOIRE
ROMANS sur ISERE

LAB - F - 75 Rév.9
Logiciel L511420
Tél. 04 75 05 60 00
Poste 6319

Numéro: 186507   Révision: 0

Terres rares

Dy	<	0.06		µg/g UO2	MDS		BMY	511231
DyEuSmGd	=	0.24		µg/g UO2	MDS	Conforme	BMY	
Eu	=	0.04	+-0.04	µg/g UO2	MDS		BMY	511231
Gd	<	0.06		µg/g UO2	MDS		BMY	511231
Sm	<	0.08		µg/g UO2	MDS		BMY	511231

Test de frittabilité

Compression	=	2.95	T/cm2	GRT		CIT
Essai Brés.	=	21.2	daN	GRT		CIT
Frittabilité	=	98.10	% d.th.	GRT	Conforme	CIT
Aspect	=	20		GRT	Conforme	CIT
Observations	=	Accepté		GRT		CIT